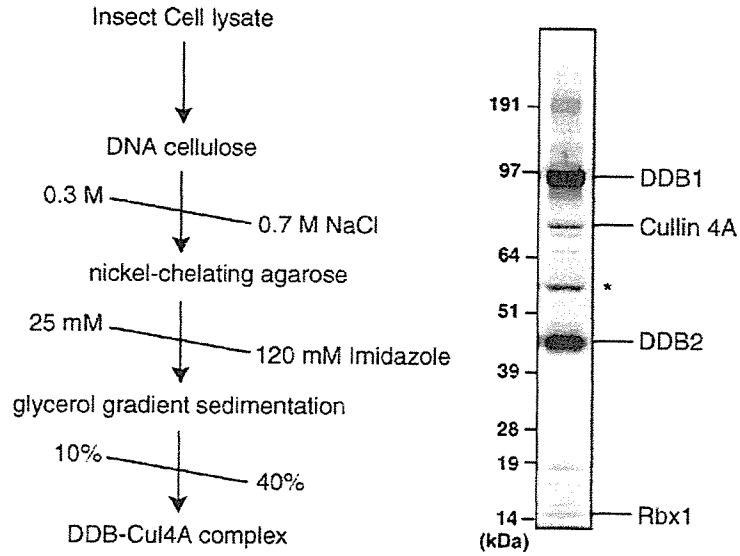

Fig. 2. Purification of the baculovirus-expressed DDB–Cul4A complex. The DDB–Cul4A complex was purified by sequential column chromatography and subsequently separated onto a 10–40% glycerol gradient by ultracentrifugation. The peak fraction of DDB–Cul4A complex was resolved by SDS-PAGE and visualized by silver staining. Asterisk shows the contaminant protein (see Section 3).

nal of DDB1 was fainter than that of Cul4A and DDB2 (see Section 4).

To further investigate the biochemical characteristics of DDB–Cul4A complex, we next purified it under more physiological conditions. HeLa cells stably expressing FLAG-HA-tagged DDB2 [17] were used to collect E3 complex. The DDB2-containing complex was immunoprecipitated with anti-FLAG antibody followed by anti-HA antibody as described previously [17] and the eluates were further purified by Mini Q column chromatography. The authentic E3 complex, comprised of DDB1, DDB2, Cul4A and Rbx1, was purified to almost homogeneity (Fig. 4A). When this complex was incubated with ATP, ubiquitin, E1 and UbcH5a, apparent high molecular-mass ladders derived from the ubiquity-

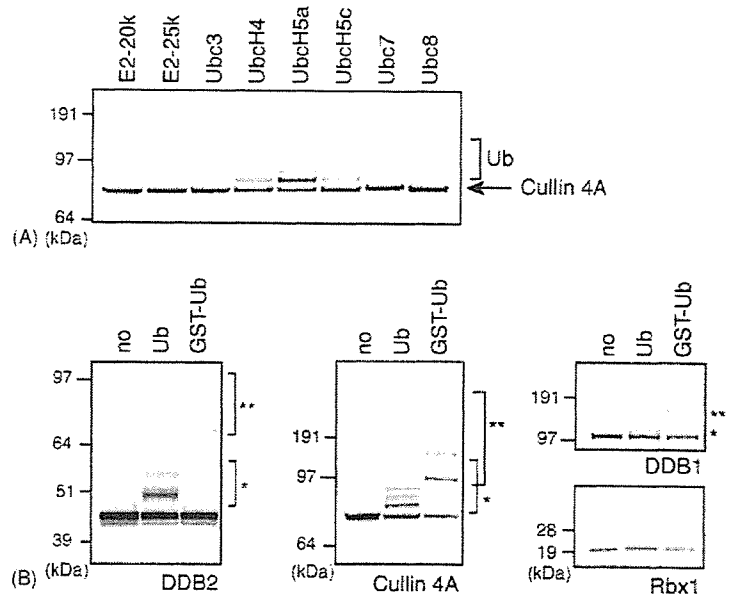

Fig. 3. In vitro reconstitution of DDB2 ubiquitylation. (A) The DDB–Cul4A E3 complex cooperates with Ubc4 and UbcH5 subfamily of E2 enzymes. Purified DDB–Cul4A E3 was incubated with the indicated E2 enzymes and subjected to immunoblotting with anti-HA antibody to identify the auto-ubiquitylation. (B) DDB2 was directly ubiquitylated by the DDB–Cul4A complex. Pure DDB1–DDB2-Cul4A complex was subjected to in vitro ubiquitylation assay in the absence (no) or presence of ubiquitin (Ub) or GST-ubiquitin (GST-Ub) and analyzed by immunoblotting with each antibody. Single asterisks show the ubiquitin conjugation and double asterisks indicate GST-ubiquitin conjugation.

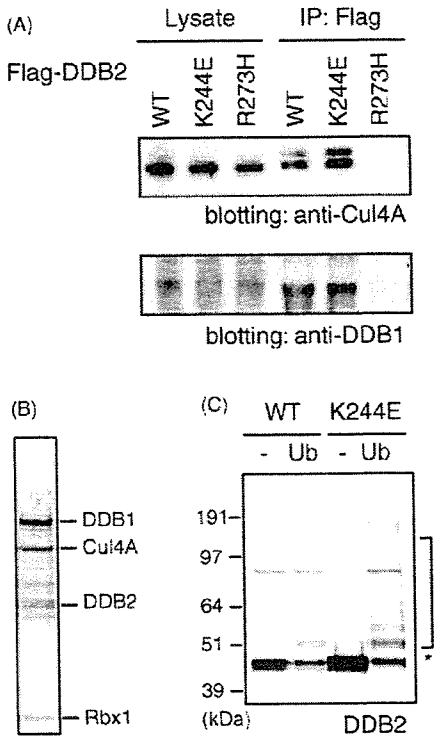

Fig. 5. XP82TO mutation (K244E) does not affect the in vitro ubiquitylation of DDB2. (A) DDB2-K244E interacts with DDB1 and Cul4A, but DDB2-R273H associates with neither. Flag-DDB2 (WT, K244E or R273H) was co-transfected with Myc-Cul4A and HA-DDB1 into ts41 cells. After immunoprecipitation (IP) by anti-Flag antibody, the resulting immunoprecipitates were subjected to immunoblotting using anti-Cul4A and anti-DDB1 antibodies. (B) The DDB2 (K244E) complex was resolved by SDS-PAGE and visualized by silver staining. (C) Ubiquitylation of DDB2 protein with XP-E mutation (DDB2-K244E) was comparable with that of wild-type DDB2 in vitro. The DDB–Cul4A complex containing mutant or wild type DDB2 was subjected to in vitro ubiquitylation in the presence (Ub) or absence (-) of ubiquitin. Asterisk indicates the ubiquitin-conjugated DDB2.

Interestingly, ectopic over-production of Cullin 4A accelerates the degradation of DDB2, suggesting that Cul4A ubiquitylates DDB2 [15,16]. However, no reconstitution experiments were performed and thus this information did not exclude the possible involvement of other E3(s) downstream of Cul4A in the ubiquitylation of DDB2, rather than directly by Cul4A. This situation prompted us to reconstitute the in vitro ubiquitylation of DDB2 and we presented in this study biochemical evidence for the ubiquitylation of DDB2 directly by the DDB–Cullin 4A complex.

4.1. In vitro ubiquitylation of each subunit of the DDB complex

It is well established that a significant fraction of DDB2 is degraded promptly after UV irradiation [21,22] and is also degraded in a cell cycle-dependent manner [16]. Conversely, it is still controversial whether another component of the DDB complex, DDB1, is a target of ubiquitylation and subsequent degradation. Zhou's group reported that overproduction of Cul4A in cells stimulates the ubiquitylation of DDB1 [15]. In contrast, neither ectopically expressed Cul4A nor UV irradiation accelerates degradation of DDB1 was reported by other groups [12,16]. In our reconstitution experiment, DDB1 was very weakly ubiquitylated in the DDB–Cul4A complex from insect cells (Fig. 3B) and seldom ubiquitylated in the complex from HeLa cells (Fig. 4B). Because the HeLa cell-derived complex is purer and was considered to be isolated under more physiological conditions, this result supports the notion that DDB1 is not ubiquitylated by the Cul4A E3 complex. Even though DDB1 was faintly ubiquitylated, such mono- or di-ubiquitylation is insufficient for the proteasomal degradation. Therefore, we favor the scenario that not DDB1 but DDB2 is the target of ubiquitylation by Cul4A E3 complex in vivo [12,16].

4.2. XP-E mutation did not affect the ubiquitylation of p48 in vitro

Rapic-Otrin et al. [21] reported that UV-induced rapid degradation of DDB2 did not occur in the XP-E cell line (XP82TO) whose DDB2 harbors a K244E mutation. Because this mutant protein (DDB2-K244E) can interact with DDB1 and Cullin 4A (Fig. 5A [13]) but not with damaged DNA [8,12,34], this result suggests that the binding activity to damaged-DNA is necessary for the degradation of DDB2. Another possibility is that the mutated site of DDB2 (244th K) per se is the main ubiquitylation site, as suggested previously [21]. However, the latter is unlikely because we showed that this mutant protein was still ubiquitylated in a manner similar to the wild-type DDB2 protein in vitro (Fig. 5C). Perhaps binding to damaged-DNA renders the conformation of DDB complex more acquiescent for ubiquitylation and/or UV recruits DDB to some specialized chromatin place where the other ubiquitylation machinery is easy to access in vivo.

4.3. Biochemical role of DDB in nucleotide excision repair

In XP-E cells lacking the DDB activity, the nucleotide excision repair (NER) of cyclobutane pyrimidine dimer (CPD) is significantly impaired [32], suggesting the importance of DDB complex in NER in vivo. However, this DDB complex is not essential for the reconstitution of the cell-free NER in vitro. The NER reaction was successfully reconstituted in the absence of DDB [35–37], although it may exhibit some stimulatory or inhibitory effects under certain conditions [38–40]. One interpretation of these results is that some partner protein(s) of DDB complex may be missing in such NER assay in vitro. Recent studies [13,15–20,41–43] and the present work emphasize the role of the DDB1 complex in the ubiquitin ligation. We can thus speculate that the effect and requirement of DDB could change if other ubiquitylation machinery was added to the in vitro NER assay.

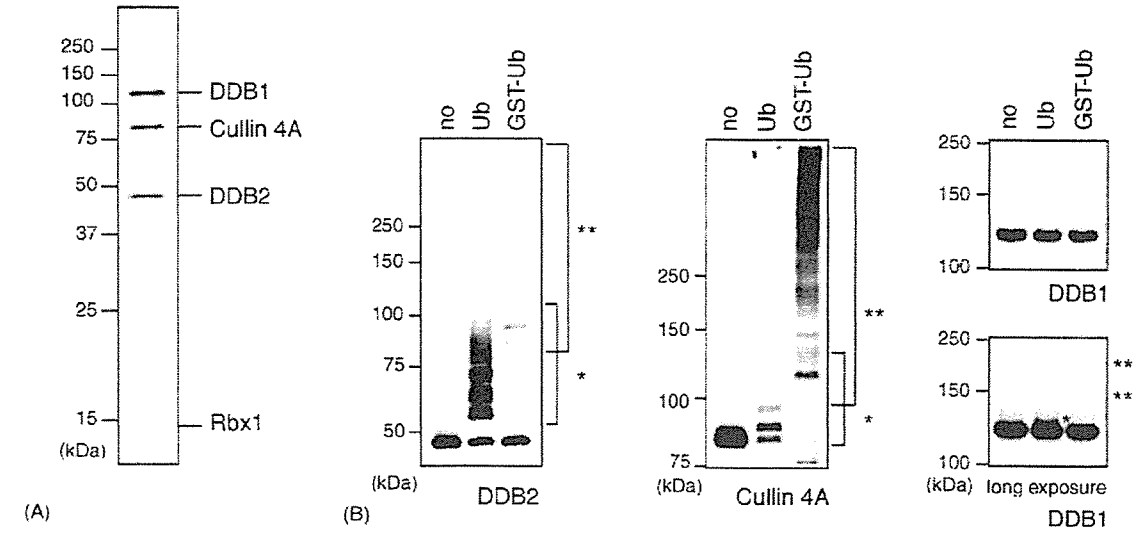

Fig. 4. In vitro ubiquitylation of DDB2 using authentic DDB–Cul4A complex. (A) Purification of the genuine DDB–Cul4A complex. Purified complex was resolved by SDS-PAGE and visualized by silver staining. (B) In vitro ubiquitylation of DDB2 and auto-ubiquitylation of Cul4A. The authentic DDB–Cul4A complex was subjected to in vitro ubiquitylation assay in the absence (no) or presence of ubiquitin (Ub) or GST-ubiquitin (GST-Ub) and analyzed by immunoblotting with anti-HA (DDB2), anti-Cul4A and anti-DDB1 antibodies. Single asterisks show the ubiquitin conjugation and double asterisks indicate GST-ubiquitin conjugation.

lation of DDB2 and Cul4A were again observed (Fig. 4B, single asterisk). The exclusion of ubiquitin from the assay quenched these bands and replacement of native ubiquitin with GST-ubiquitin retarded their mobility (Fig. 4B, double asterisks). In contrast, DDB1 was rarely ubiquitylated, although a faint ubiquitylation signal was observed after long exposure (Fig. 4B, right panel). Because the DDB–Cul4A complex derived from both insect (Fig. 3) and mammalian (Fig. 4) cells directly ubiquitylated DDB2, we concluded that DDB2 was ubiquitylated by genuine DDB–Cul4A complex.

3.4. XP-E mutation does not affect ubiquitylation of DDB2 in vitro

Two cell lines established from XP-E patients, XP2RO and XP82TO, have been characterized in detail. XP2RO and XP82TO cells harbor naturally occurring single amino acid substitutions, R273H and K244E, in DDB2 protein, respectively. It has been reported that the XP82TO mutant protein (DDB2-K244E) interacts normally with DDB1 and Cullin 4A. Conversely, XP2RO mutant protein (DDB2-R273H) interacts with neither of them [13,29]. We also confirmed by immunoprecipitation experiments that DDB2-K244E interacts with DDB1 and Cullin 4A normally, but DDB2-R273H did not associate with either of them (Fig. 5A). Intriguingly, Rapic-Otrin et al. [21] reported that UV-induced rapid degradation of DDB2 protein did not occur in XP82TO cell line. This information prompted us to test whether K244E mutation affects the in vitro ubiquitylation of DDB2. Because DDB1–DDB2 (K244E)-Cul4A complex did not interact effectively with DNA cellulose, we were unable to purify it compared with the wild-type complex (data not shown). We thus purified this mutant protein complex by affinity chromatography on nickel-chelating column and subsequent heparin column, and the bound DDB2 (K244E) complex was eluted around 0.5 M NaCl (Fig. 5B). As a control, the wild type DDB2-containing complex was simultaneously isolated by the same method. The DDB1–DDB2 (K244E)-Cul4A complex was incubated with ATP, ubiquitin, E1 and UbcH5a, and subjected to immunoblotting with the anti-Flag antibody. The mutant DDB2 protein was ubiquitylated in a manner equivalent to that of the wild-type control (Fig. 5C), indicating that XP82TO mutation (K244E) did not affect the ubiquitylation of DDB2 in vitro. This result also suggests that the mutated site of DDB2 (244th K) per se is not the unique ubiquitylation site.

4. Discussion

The DDB complex is regulated through several processes when cells are exposed to UV irradiation, namely very rapid translocation into the nucleus and binding to chromatin [17,29–31], hasty degradation of DDB2 protein [21,22] and final transcriptional induction of *DDB2* mRNA [32,33]. Chemical inhibition of proteasomes prevents rapid degradation of DDB2 protein, suggesting that this process is mediated by the ubiquitin/proteasome system. Among these regulation processes of DDB2, proteolytic degradation is the most intriguing because several recent reports [13,15–17] and our present results have shown a tight relationship between the DDB complex and proteins involved in ubiquitylation.

4.4. Biological function of DDB2 ubiquitylation

As mentioned above, DDB2 protein is rapidly degraded after UV-irradiation in vivo [21,22] and we showed here that the DDB–Cul4A complex could directly ubiquitylate DDB2. What is the function of DDB2 ubiquitylation and subsequent degradation? After damaged-DNA recognition, DDB is thought to hand over the DNA lesion to the following NER component(s) including XPC [2]. An appealing hypothesis is that clearance of DDB2 by ubiquitylation and succeeding degradation facilitates accession of the following NER factor(s) to the DNA lesion. However, it is not clear at present whether the ubiquitylation of DDB2 is only required for its UV-induced degradation, or is essential to change some biological character of DDB2 preceding degradation. Because various non-proteolytic functions of ubiquitylation have been identified recently [44], it is still conceivable that the ubiquitylation of DDB2 might have an additional role besides degradation. Moreover, we still do not know whether DDB2 ubiquitylation is a pertinent event for DDB function in DNA repair, or is the only side effect accompanied by ubiquitylation of authentic, relevant substrate. To define the precise role of DDB–Cullin 4A complex-mediated ubiquitylation, further studies are obviously required; especially the identification of the physiological substrate. Such experiments are currently underway in our laboratories.

Acknowledgements

We are grateful to Dr. Yoshihiro Nakatani of Harvard Medical School for providing HeLa cells expressing epitope-tagged DDB2 and to Dr. Kaoru Sugasawa of RIKEN for the critical reading of the manuscript. We also thank all members of Prof. K. Tanaka laboratory for the helpful discussions. This work was supported by CREST of Japan Science and Technology (JST), Takeda Science Foundation (to M.S.) and Grants-in-Aid from the Ministry of Education, Culture, Sports, Science and Technology of Japan (to K.T.).

References

[1] R.S. Feldberg, L. Grossman, A DNA binding protein from human placenta specific for ultraviolet damaged DNA, Biochemistry 15 (1976) 2402–2408.
[2] J. Tang, G. Chu, Xeroderma pigmentosum complementation group E and UV-damaged DNA-binding protein, DNA Repair 1 (2002) 601–616.
[3] B.B.O. Wittschieben, R.D. Wood, DDB complexities, DNA Repair 2 (2003) 1065–1069.
[4] D. Bootsma, K.H. Kraemer, J.E. Cleaver, J.H.J. Hoeijmakers, Nucleotide excision repair syndromes: xeroderma pigmentosum, Cockayne syndrome and trichothiodystrophy, in: B. Vogelstein, K.W. Kinzler (Eds.), The Genetic Basis of Human Cancer, McGraw Hill, New York, 1997, pp. 245–274.
[5] G. Chu, E. Chang, Xeroderma pigmentosum group E cells lack a nuclear factor that binds to damaged DNA, Science 242 (1988) 564–567.
[6] B.J. Hwang, S. Toering, U. Francke, G. Chu, p48 activates a UV-damaged-DNA binding factor and is defective in xeroderma pigmentosum group E cells that lack binding activity, Mol. Cell. Biol. 18 (1998) 4391–4399.
[7] S. Keeney, A.P. Eker, T. Brody, W. Vermeulen, D. Bootsma, J.H. Hoeijmakers, S. Linn, Correction of the DNA repair defect in xeroderma pigmentosum group E by injection of a DNA damage-binding protein, Proc. Natl. Acad. Sci. U.S.A. 91 (1994) 4053–4056.
[8] V. Rapic-Otrin, I. Kuraoka, T. Nardo, M. McLenigan, A.P. Eker, M. Stefanini, A.S. Levine, R.D. Wood, Relationship of the xeroderma pigmentosum group E DNA repair defect to the chromatin and DNA binding proteins UV-DDB and replication protein A, Mol. Cell. Biol. 18 (1998) 3182–3190.
[9] J.Y. Tang, B.J. Hwang, J.M. Ford, P.C. Hanawalt, G. Chu, Xeroderma pigmentosum p48 gene enhances global genomic repair and suppresses UV-induced mutagenesis, Mol. Cells 5 (2000) 737–744.
[10] A.F. Nichols, P. Ong, S. Linn, Mutations specific to the xeroderma pigmentosum group E Ddb-phenotype, J. Biol. Chem. 271 (1996) 24317–24320.
[11] T. Itoh, S. Linn, T. Ono, M. Yamaizumi, Reinvestigation of the classification of five cell strains of xeroderma pigmentosum group E with reclassification of three of them, J. Invest. Dermatol. 114 (2000) 1022–1029.
[12] V. Rapic-Otrin, V. Navazza, T. Nardo, E. Botta, M. McLenigan, D.C. Bisi, A.S. Levine, M. Stefanini, True XP group E patients have a defective UV-damaged DNA binding protein complex and mutations in DDB2 which reveal the functional domains of its p48 product, Hum. Mol. Genet. 12 (2003) 1507–1522.
[13] P. Shiyanov, A. Nag, P. Raychaudhuri, Cullin 4A associates with the UV-damaged DNA-binding protein DDB, J. Biol. Chem. 274 (1999) 35309–35312.
[14] N. Zheng, B.A. Schulman, L. Song, J.J. Miller, P.D. Jeffrey, P. Wang, C. Chu, D.M. Koepp, S.J. Elledge, M. Pagano, R.C. Conaway, J.W. Conaway, J.W. Harper, N.P. Pavletich, Structure of the Cul1-Rbx1-Skp1-F boxSkp2 SCF ubiquitin ligase complex, Nature 416 (2002) 703–709.
[15] X. Chen, Y. Zhang, L. Douglas, P. Zhou, UV-damaged DNA-binding proteins are targets of CUL-4A-mediated ubiquitination and degradation, J. Biol. Chem. 276 (2001) 48175–48182.
[16] A. Nag, T. Bondar, S. Shiv, P. Raychaudhuri, The xeroderma pigmentosum group E gene product DDB2 is a specific target of cullin 4A in mammalian cells, Mol. Cell. Biol. 21 (2001) 6738–6747.
[17] R. Groisman, J. Polanowska, I. Kuraoka, J. Sawada, M. Saijo, R. Drapkin, A.F. Kisselev, K. Tanaka, Y. Nakatani, The ubiquitin ligase activity in the DDB2 and CSA complexes is differentially regulated by the COP9 signalosome in response to DNA damage, Cell 113 (2003) 357–367.
[18] C. Liu, K.A. Powell, K. Mundt, L. Wu, A.M. Carr, T. Caspari, Cop9/signalosome subunits and Pcu4 regulate ribonucleotide reductase by both checkpoint-dependent and -independent mechanisms, Genes Dev. 17 (2003) 1130–1140.
[19] T. Bondar, A. Ponomarev, P. Raychaudhuri, Ddb1 is required for the proteolysis of the *Schizosaccharomyces pombe* replication inhibitor Spd1 during S phase and after DNA damage, J. Biol. Chem. 279 (2004) 9937–9943.
[20] I.E. Wertz, K.M. O'Rourke, Z. Zhang, D. Dornan, D. Arnott, R.J. Deshaies, V.M. Dixit, Human De-etiolated-1 regulates c-Jun by assembling a CUL4A ubiquitin ligase, Science 303 (2004) 1371–1374.
[21] V. Rapic-Otrin, M.P. McLenigan, D.C. Bisi, M. Gonzalez, A.S. Levine, Sequential binding of UV DNA damage binding factor and degradation of the p48 subunit as early events after UV irradiation, Nucleic Acids Res. 30 (2002) 2588–2598.
[22] M.E. Fitch, I.V. Cross, S.J. Turner, S. Adimoolam, C.X. Lin, K.G. Williams, J.M. Ford, The DDB2 nucleotide excision repair gene product p48 enhances global genomic repair in p53 deficient human fibroblasts, DNA Repair 2 (2003) 819–826.

[23] T. Natsume, Y. Yamauchi, H. Nakayama, T. Shinkawa, M. Yanagida, N. Takahashi, T. Isobe, A direct nanoflow liquid chromatography-tandem mass spectrometry system for interaction proteomics, Anal. Chem. 74 (2002) 4725–4733.

[24] M. Komatsu, T. Chiba, K. Tatsumi, S.-I. Iemura, I. Tanida, N. Okazaki, T. Ueno, E. Kominami, T. Natsume, K. Tanaka, A novel protein-conjugating system for Ufm1, a ubiquitin-fold modifier, EMBO J. 23 (2004) 1977–1986.

[25] S. Handeli, H. Weintraub, The ts41 mutation in Chinese hamster cells leads to successive S phases in the absence of intervening G2, M, and G1, Cell 71 (1992) 599–611.

[26] N. Matsuda, T. Suzuki, K. Tanaka, A. Nakano, Rma1, a novel type of RING finger protein conserved from Arabidopsis to human, is a membrane-bound ubiquitin ligase, J. Cell Sci. 114 (2001) 1949–1957.

[27] N. Imai, N. Matsuda, K. Tanaka, A. Nakano, S. Matsumoto, W. Kang, Ubiquitin ligase activities of Bombyx mori nucleopolyhedrovirus RING finger proteins, J. Virol. 77 (2003) 923–930.

[28] L.C. Chen, S. Manjeshwar, Y. Lu, D. Moore, B.M. Ljung, W.L. Kuo, S.H. Dairkee, M. Wernick, C. Collins, H.S. Smith, The human homologue for the *Caenorhabditis elegans* cul-4 gene is amplified and overexpressed in primary breast cancers, Cancer Res. 58 (1998) 3677–3683.

[29] P. Shiyanov, S.A. Hayes, M. Donepudi, A.F. Nichols, S. Linn, B.L. Slagle, P. Raychaudhuri, The naturally occurring mutants of DDB are impaired in stimulating nuclear import of the p125 subunit and E2F1-activated transcription, Mol. Cell. Biol. 19 (1999) 4935–4943.

[30] V. Rapic-Otrin, M. McLenigan, M. Takao, A.S. Levine, M. Protic, Translocation of a UV-damaged DNA binding protein into a tight association with chromatin after treatment of mammalian cells with UV light, J. Cell Sci. 110 (1997) 1159–1168.

[31] W. Liu, A.F. Nichols, J.A. Graham, R. Dualan, A. Abbas, S. Linn, Nuclear transport of human DDB protein induced by ultraviolet light, J. Biol. Chem. 275 (2000) 21429–21434.

[32] B.J. Hwang, J.M. Ford, P.C. Hanawalt, G. Chu, Expression of the p48 xeroderma pigmentosum gene is p53-dependent and is involved in global genomic repair, Proc. Natl. Acad. Sci. U.S.A. 96 (1999) 424–428.

[33] T. Itoh, C. O'Shea, S. Linn, Impaired regulation of tumor suppressor p53 caused by mutations in the xeroderma pigmentosum DDB2 gene: mutual regulatory interactions between p48(DDB2) and p53, Mol. Cell. Biol. 23 (2003) 7540–7553.

[34] S. Keeney, H. Wein, S. Linn, Biochemical heterogeneity in xeroderma pigmentosum complementation group E, Mutat. Res. 273 (1992) 49–56.

[35] M. Araki, C. Masutani, T. Maekawa, Y. Watanabe, A. Yamada, R. Kusumoto, D. Sakai, K. Sugasawa, Y. Ohkuma, F. Hanaoka, Reconstitution of damage DNA excision reaction from SV40 minichromosomes with purified nucleotide excision repair proteins, Mutat. Res. 459 (2000) 147–160.

[36] S.J. Araujo, F. Tirode, F. Coin, H. Pospiech, J.E. Syvaoja, M. Stucki, U. Hubscher, J.M. Egly, R.D. Wood, Nucleotide excision repair of DNA with recombinant human proteins: definition of the minimal set of factors, active forms of TFIIH, and modulation by CAK, Genes Dev. 14 (2000) 349–359.

[37] D. Mu, C.H. Park, T. Matsunaga, D.S. Hsu, J.T. Reardon, A. Sancar, Reconstitution of human DNA repair excision nuclease in a highly defined system, J. Biol. Chem. 270 (1995) 2415–2418.

[38] A. Aboussekhra, M. Biggerstaff, M.K. Shivji, J.A. Vilpo, V. Moncollin, V.N. Podust, M. Protic, U. Hubscher, J.M. Egly, R.D. Wood, Mammalian DNA nucleotide excision repair reconstituted with purified protein components, Cell 80 (1995) 859–868.

[39] M. Wakasugi, M. Shimizu, H. Morioka, S. Linn, O. Nikaido, T. Matsunaga, Damaged DNA-binding protein DDB stimulates the excision of cyclobutane pyrimidine dimers in vitro in concert with XPA and replication protein A, J. Biol. Chem. 276 (2001) 15434–15440.

[40] M. Wakasugi, A. Kawashima, H. Morioka, S. Linn, A. Sancar, T. Mori, O. Nikaido, T. Matsunaga, DDB accumulates at DNA damage sites immediately after UV irradiation and directly stimulates nucleotide excision repair, J. Biol. Chem. 277 (2002) 1637–1640.

[41] Y. Yanagawa, J.A. Sullivan, S. Komatsu, G. Gusmaroli, G. Suzuki, J. Yin, T. Ishibashi, Y. Saijo, V. Rubio, S. Kimura, J. Wang, X.W. Deng, Arabidopsis COP10 forms a complex with DDB1 and DET1 in vivo and enhances the activity of ubiquitin conjugating enzymes, Genes Dev. 18 (2004) 2172–2181.

[42] L.A. Higa, I.S. Mihaylov, D.P. Banks, J. Zheng, H. Zhang, Radiation-mediated proteolysis of CDT1 by CUL4-ROC1 and CSN complexes constitutes a new checkpoint, Nat. Cell Biol. 5 (2003) 1008–1015.

[43] J. Hu, C.M. McCall, T. Ohta, Y. Xiong, Targeted ubiquitination of CDT1 by the DDB1–CUL4A-ROC1 ligase in response to DNA damage, Nat. Cell Biol. 6 (2004) 1003–1009.

[44] J.D. Schnell, L. Hicke, Non-traditional functions of ubiquitin and ubiquitin-binding proteins, J. Biol. Chem. 278 (2003) 35857–35860.

THE JOURNAL OF BIOLOGICAL CHEMISTRY VOL. 280, NO. 52, pp. 42685–42693, December 30, 2005

WNK1 Regulates Phosphorylation of Cation-Chloride-coupled Cotransporters via the STE20-related Kinases, SPAK and OSR1*[S]

Received for publication, September 13, 2005, and in revised form, October 27, 2005 Published, JBC Papers in Press, October 31, 2005, DOI 10.1074/jbc.M510042200

Tetsuo Moriguchi[‡§], Seiichi Urushiyama[‡], Naoki Hisamoto[¶], Shun-ichiro Iemura[‖], Shinichi Uchida[**], Tohru Natsume[‖], Kunihiro Matsumoto[¶], and Hiroshi Shibuya[‡§1]

From the [‡]Department of Molecular Cell Biology, Medical Research Institute and School of Biomedical Science, Tokyo Medical and Dental University, and CREST, JST, Chiyoda, Tokyo 101-0062, the [§]Center of Excellence Program for Frontier Research on Molecular Destruction and Reconstruction of Tooth and Bone, Kanda-Surugadai, Chiyoda, Tokyo 101-0062, the [¶]Department of Molecular Biology, Graduate School of Science, Nagoya University and CREST, JST, Chikusa-ku, Nagoya 464-8602, the [‖]National Institutes of Advanced Industrial Science and Technology, Biological Information Research Center (JBIRC), Kohtoh-ku, Tokyo 135-0064, and the [**]Department of Nephrology, Graduate School of Medicine, Tokyo Medical and Dental University, Bunkyo, Tokyo 113-8519, Japan

The WNK1 and WNK4 genes have been found to be mutated in some patients with hyperkalemia and hypertension caused by pseudohypoaldosteronism type II. The clue to the pathophysiology of pseudohypoaldosteronism type II was its striking therapeutic response to thiazide diuretics, which are known to block the sodium chloride cotransporter (NCC). Although this suggests a role for WNK1 in hypertension, the precise molecular mechanisms are largely unknown. Here we have shown that WNK1 phosphorylates and regulates the STE20-related kinases, Ste20-related proline-alanine-rich kinase (SPAK) and oxidative stress response 1 (OSR1). WNK1 was observed to phosphorylate the evolutionary conserved serine residue located outside the kinase domains of SPAK and OSR1, and mutation of the OSR1 serine residue caused enhanced OSR1 kinase activity. In addition, hypotonic stress was shown to activate SPAK and OSR1 and induce phosphorylation of the conserved OSR1 serine residue, suggesting that WNK1 may be an activator of the SPAK and OSR1 kinases. Moreover, SPAK and OSR1 were found to directly phosphorylate the N-terminal regulatory regions of cation-chloride-coupled cotransporters including NKCC1, NKCC2, and NCC. Phosphorylation of NCC was induced by hypotonic stress in cells. These results suggested that WNK1 and SPAK/OSR1 mediate the hypotonic stress signaling pathway to the transporters and may provide insights into the mechanisms by which WNK1 regulates ion balance.

WNK[2] kinases (with no lysine (K)) comprise a family of novel serine/threonine protein kinases conserved among multicellular organisms (1, 2). The kinase domain of this family is unique in that it lacks the conserved lysine residue previously known to be important for ATP binding in the catalytic site. A conserved lysine in subdomain I of the WNK kinases is thought to be essential for their catalytic activity (1, 3). There are four human WNK family members. *WNK1* and *WNK4* were identified as genes mutated in families of patients with pseudohypoaldosteronism type 2 (PHA II) human hypertension (4). The *WNK1* gene mutation consists of a deletion within its first intron, leading to increased expression, whereas mutations in the *WNK4* gene are found in the coding sequence near the coiled-coil domains.

PHA II patients are treated by thiazide diuretics, which function as antagonists of the Na-Cl cotransporter (NCC, also known as thiazide-sensitive cotransporter (TSC) or Na-Cl transporter (NCCT)), suggesting that the activity of NCC could be potentially involved in the development of PHA II. Previous studies using *Xenopus* oocytes have showed that wild-type WNK4 inhibits the surface expression and the activity of NCC, whereas one of the disease-causing mutants of WNK4 attenuated this inhibitory effect (5, 6). However, comparison of wild-type and mutant WNK4 revealed no differences in NCC surface expression in polarized epithelial cells (MDCK II cells), suggesting that the regulation of intracellular NCC localization by WNK4 might be unrelated to the pathogenesis of PHA II (7). WNK4 has also been reported to inhibit surface expression of the secretory potassium channel (ROMK) and Cl^- base exchanger SCL26A6 (CFEX), in addition to NCC, in *Xenopus* oocytes (8, 9). Furthermore, the disease-causing mutant of WNK4 was shown to increase paracellular chloride permeability in MDCK cells (10, 11). In contrast to WNK4, little is known about the functions and regulation of WNK1. WNK1 does not directly affect NCC activity in *Xenopus* oocytes but has been shown to modulate the inhibitory effects of WNK4 on NCC (6). Although WNK1 activates the MEK5-ERK5 pathway and phosphorylates synaptotagmin, there is no direct evidence to link WNK1 and transporter function (12, 13). Moreover, a recent study reported that WNK1 regulates the epithelial sodium channel through glucocorticoid-inducible kinase (SGK1), but the mechanisms of SGK1 activation by WNK1 have not been fully elucidated (14, 15).

NCC contains 12 transmembrane domains and is closely related to the Na-K-2Cl cotransporters, NKCC1 and NKCC2 (16–18). NCC and NKCC2 are expressed in the kidney and function in renal salt reabsorption, whereas NKCC1 is expressed ubiquitously and plays a key role in

* This work was supported by the Center of Excellence Program for Frontier Research on Molecular Destruction and Reconstruction of Tooth and Bone, grants-in-aid for scientific research from the Ministry of Education, Science, Sports and Culture of Japan, and grants provided by the Ichiro Kanehara Foundation, the Naito Foundation, the Yamanouchi Foundation for Research on Metabolic Disorders, and the Center of Excellence Program for Frontier Research. The costs of publication of this article were defrayed in part by the payment of page charges. This article must therefore be hereby marked "*advertisement*" in accordance with 18 U.S.C. Section 1734 solely to indicate this fact.

[S] The on-line version of this article (available at http://www.jbc.org) contains a supplemental figure showing the specificity of anti-SPAK/OSR1 and anti-OSR1-P antibodies.

[1] To whom correspondence should be addressed. Tel. and Fax: 81-3-5280-8062, E-mail: shibuya.mcb@mri.tmd.ac.jp.

[2] The abbreviations used are: WNK, with no lysine (K); NCC, Na-Cl cotransporter; KCC, K-Cl cotransporter; NKCC, Na-K-2Cl cotransporter; SPAK, Ste20-related proline-alanine-rich kinase; OSR1, oxidative stress response 1; ERK, extracellular signal-regulated kinase; MEK, mitogen-activated protein kinase/extracellular signal-regulated kinase; MS, mass spectrometry; LC-MS/MS, liquid chromatography coupled to tandem MS; GST, glutathione S-transferase; PHA II, pseudohypoaldosteronism type 2; MDCK, Madin-Darby canine kidney cells.

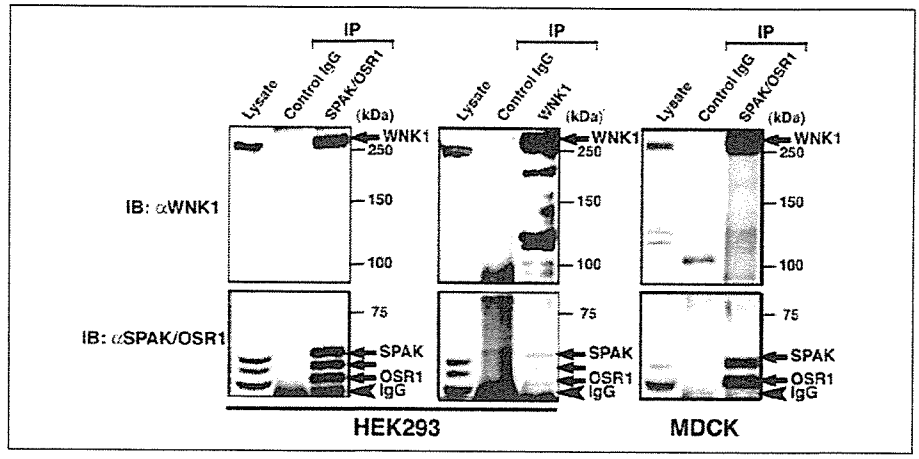

FIGURE 1. **Association of WNK1 with SPAK and OSR1.** SPAK and OSR1 were immunoprecipitated (*IP*) from 0.4 mg of lysates prepared from HEK293 cells (*left*) or MDCK cells (*right*) with 2 μg of SPAK/OSR1 antibody, fractionated by SDS-PAGE, and immunoblotted (*IB*) with the indicated antibodies. WNK1 was immunoprecipitated from 1 mg of HEK293 lysates with 10 μg of the WNK1 antibody (*middle*). As a control, immunoprecipitations were also performed in parallel experiments with rabbit IgG (Chemicon International).

epithelial salt secretion and cell volume regulation. NKCC1 cotransport activity is controlled by the phosphorylation/dephosphorylation of several threonine and serine residues in response to decreases in cell volume or intracellular [Cl]. Three of the phosphoacceptors in the N terminus of NKCC1 have been identified, and the amino acid sequences surrounding these residues are highly conserved among the members of the cation-chloride-coupled cotransporter family, suggesting that phospho-regulatory mechanisms are conserved among these cotransporters (19). Although several protein kinases, such as SGK1 and c-Jun N-terminal kinase, have been proposed as candidates for the activators of NKCC1, there is no evidence showing that any kinase directly phosphorylates NKCC1 *in vivo* (20, 21). It has been previously reported that the STE20-related kinases, SPAK (also called PASK (proline-alanine-rich Ste-20-related kinase)) and OSR1, bind to the N-terminal regions of the cation-chloride cotransporters KCC3, NKCC1, and NKCC2 (22). Moreover, WNK4 has been identified as a putative SPAK-binding protein by yeast two-hybrid screening (23). Expression of a dominant-negative form of SPAK decreased cotransport activity and phosphorylation of NKCC1 (24). Therefore, SPAK is thought to play an important role in the regulation of NKCC1.

In this study, we have identified SPAK as a WNK1-binding protein and provided evidence that WNK1 acts as a direct activator of SPAK and OSR1. Moreover, we have shown that SPAK and OSR1 directly phosphorylate the N-terminal regulatory regions of NKCC1, NKCC2, and NCC. These results have raised the possibility that WNK1 regulates the activities of a number of transporters through SPAK/OSR1 and that this regulation contributes to the pathogenesis of hypertension.

EXPERIMENTAL PROCEDURES

Molecular Cloning and Plasmid Construction—Human WNK1, human WNK4, rat SPAK, human NKCC1, human NKCC2, mouse NCC, and mouse OSR1 coding regions were amplified by PCR using Marathon-Ready cDNA (Clontech) as templates. GST-PAK3-(65–135) expression plasmid was kindly provided by T. Akiyama (25). To construct mammalian expression vectors, pCMV-FLAG and pCMV-T7, the fragment encoding one copy of the FLAG epitope or the fragment encoding one copy of the T7 epitope was inserted into pCMV vector, respectively. Several mutant cDNAs encoding WNK1, WNK4, SPAK, OSR1, NKCC1-(1–289), NKCC2-(1–181), or NCC were generated by polymerase chain reaction and subcloned into the pCMV-FLAG, pCMV-T7, pGEX4T-1, or pGEX4T-3 as indicated. The accuracy of all clones was verified by DNA sequencing.

Yeast Two-hybrid Screening and MS/MS Analysis—Full-length human WNK1 was fused to the GAL4 DNA-binding domain, and yeast two-hybrid screening was performed as described (26). LC-MS/MS analysis was performed as described previously (27). Briefly, FLAG-WNK1 was expressed in HEK293 cells and immunoprecipitated by anti-FLAG antibody. The immunocomplexes were eluted with a FLAG peptide and then digested with *Achromobacter* protease I, and the resulting peptides were analyzed using a nanoscale LC-MS/MS system.

Antibodies—Antibody to WNK1 was generated with a peptide corresponding to the N-terminal 18 amino acids of human WNK1. Anti-SPAK/OSR1 antibody was prepared by immunizing rabbits with a keyhole limpet hemocyanin-conjugated synthetic peptide (RAKKVRRVPGSSG, amino acids 362–374 of human SPAK and amino acids 314–326 of human OSR1). Anti-phospho OSR1 polyclonal antibody was produced in rabbit by immunizing with a keyhole limpet hemocyanin-conjugated synthetic phosphopeptide corresponding to residues 319–332 of OSR1 (RRVPGS (pS) GRLHKTE). The serum was affinity-purified with phosphopeptide- and the non-phosphopeptide-conjugated cellulose. Monoclonal antibodies against FLAG and T7 were purchased from Sigma and Novagen, respectively.

Immunoprecipitation and Immunoblotting—HEK293 and MDCK cells were cultured in Dulbecco's modified Eagle's medium with standard supplements. HEK293 cells were transfected with the indicated plasmids by the calcium phosphate precipitation method at 50–80% confluence. After 24 h after transfection, cells were lysed in 1% Triton X-100 lysis buffer (50 mM Tris-HCl, pH 7.5, 150 mM NaCl, 1 mM EGTA, 1 mM EDTA, 1% Triton X-100, 1 mM orthovanadate, 50 mM sodium fluoride, 1 mM phenylmethylsulfonyl fluoride, 1 μg/ml aprotinin, 1 mM dithiothreitol, 0.27 M sucrose). Protein complexes were immunoprecipitated with the indicated antibodies according to standard procedures. Isolated protein complexes were separated by SDS-PAGE and transferred to polyvinylidene fluoride membranes (Hybond-P, Amersham Biosciences). Blots were probed with the indicated antibodies, and bound antibodies were visualized using horseradish peroxidase-conjugated secondary antibodies (Amersham Biosciences) and Western Lightning chemiluminescence reagent Plus (PerkinElmer Life Sciences) according to standard procedures. For ^{32}P labeling, transfected cells were incubated for 6 h with [^{32}P]phosphate (1 mCi/ml) and then lysed as described above.

Expression of GST-tagged Fusion Proteins in Escherichia coli—The pGEX constructs were transformed into *E. coli* BL21 cells, and a 0.5-liter culture was grown at 37 °C to an A_{600} of 0.8. Isopropyl-D-galactosidase was added to final 0.2 mM to induce protein expression, and the cells were cultured for another 16 h at 20 °C. Cells were harvested by centrifugation and lysed by freeze-thawing and sonication in 1% Triton X-100 lysis buffer. Glutathione *S*-transferase (GST)-tagged proteins were puri-

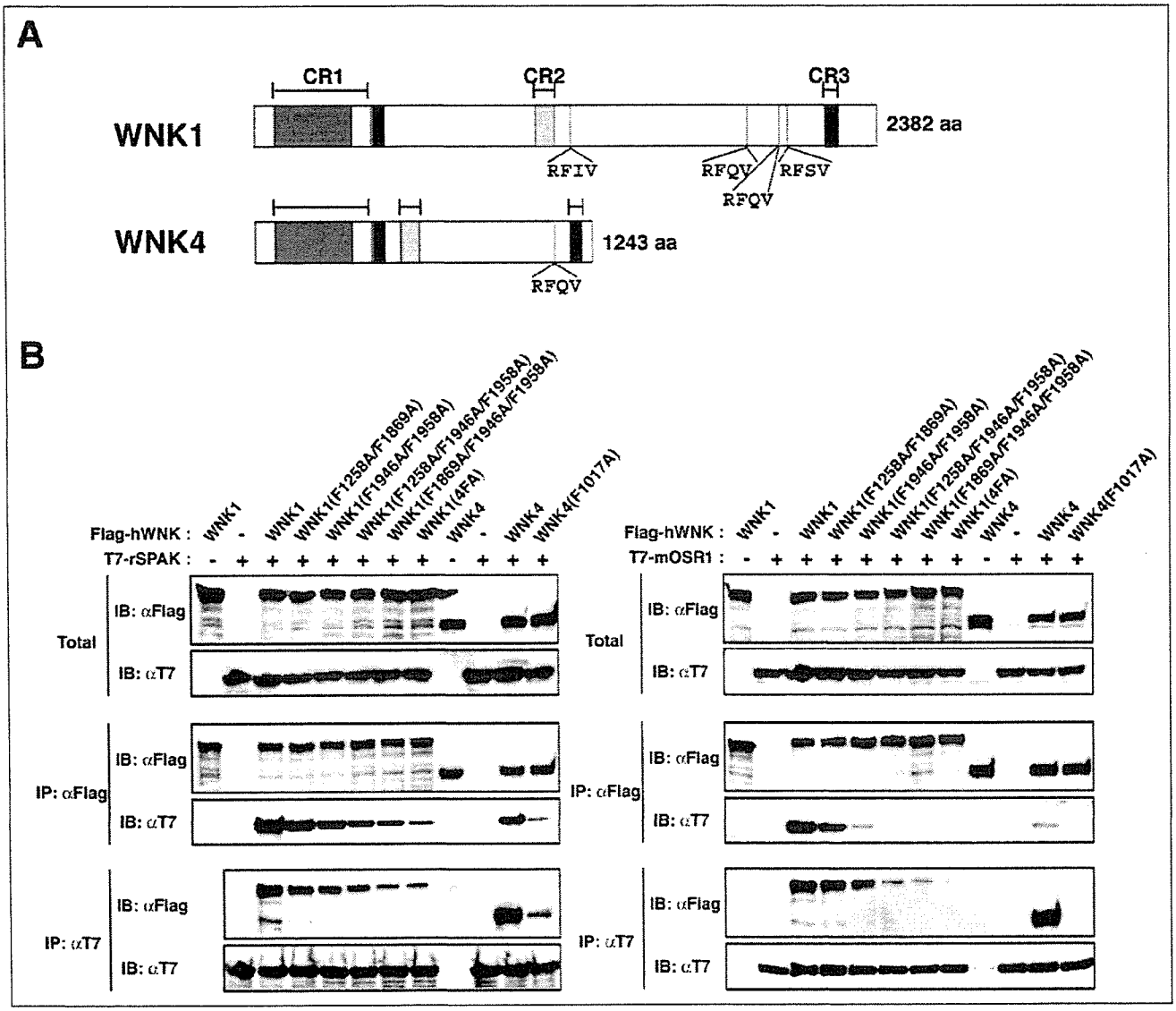

FIGURE 2. **The putative SPAK-binding motifs within WNK kinases are important for binding to SPAK and OSR1.** *A*, schematic of WNK1 and WNK4 domains. The regions of conserved homology, CR1 (kinase domain), CR2, and CR3, are indicated by *horizontal bars* above each protein. The locations of putative SPAK-binding motifs consisting of the consensus sequence (R/K-F-X-V/I) are indicated by *vertical bars*. *B*, T7-tagged rat SPAK (*left*) and mouse OSR1 (*right*, *mOSR1*) were co-transfected with various WNK1 and WNK4 mutants as indicated. Protein complexes were co-immunoprecipitated (*IP*) using either T7 antibody (*αT7*) or FLAG antibody (*αFLAG*) and then immunoblotted (*IB*) with αT7 or αFLAG. *hWNK*, human WNK.

fied from the lysates using glutathione-Sepharose and eluted from the resin in 10 mM glutathione.

Kinase Assays—Immunoprecipitated and GST-protein complexes were incubated in a kinase buffer containing 50 mM Tris-HCl, pH 7.5, 10 mM $MgCl_2$, and 100 μM [γ-^{32}P]ATP (2 μCi). After incubation for 30 min at 30 °C, the reactions were terminated by the addition of SDS sample buffer, and the proteins were separated by SDS-PAGE. Substrate phosphorylation was analyzed by autoradiography and an image analyzer (Fujix BAS 2500). For determination of phosphorylation sites by MS/MS, GST-SPAK(KM) was incubated with WNK1-(1–665) in a buffer containing 1 mM ATP for 6 h. Solutions used in hypotonic stress experiments were as follows. Basic medium contained 135 mM NaCl, 5 mM KCl, 1 mM $CaCl_2$/$MgCl_2$, 1 mM Na_2HPO_4/Na2SO4, and 15 mM sodium HEPES, pH 7.4. Low Cl^- hypotonic medium contained 67.5 mM sodium gluconate, 2.5 mM potassium gluconate, 0.5 mM $CaCl_2$/$MgCl_2$, 1 mM Na_2HPO_4/Na_2SO_4, and 7.5 mM sodium HEPES, pH 7.4.

RESULTS

Identification of the STE20-related Kinases SPAK and OSR1 as WNK1-associated Molecules—To identify a protein(s) that physically associates with WNK1, we employed two strategies: yeast two-hybrid screening and FLAG tag immunoprecipitation assays coupled with LC-MS/MS analysis. Several positive clones and putative binding proteins were identified, including STE20-like kinase SPAK. As SPAK was identified by both approaches, we analyzed it further. To investigate whether endogenous SPAK is associated with WNK1 in living cells, we generated antibodies to a peptide of SPAK (the sequence is a 100% match of the corresponding sequence of OSR1, a kinase closely related to SPAK) and a peptide of human WNK1. The anti-SPAK/OSR1 antibody reacted with three bands of 62, 60, and 58 kDa in HEK293 cell extracts and with two bands of 62 and 58 kDa in MDCK cell extracts (Fig. 1). The specificity of anti-SPAK/OSR1 antibody was confirmed by the competition

experiments using the antigen peptide used for immunization (Supplemental data, Fig. S1). The anti-WNK1 antibody reacted with a band of ~250 kDa in several cell lines (Fig. 1). We subjected a lysate from HEK293 cells to immunoprecipitation with anti-WNK1 antibody and then immunoblotted the precipitates with anti-SPAK/OSR1 antibody. SPAK and OSR1 were found to coprecipitate with WNK1 (Fig. 1, *middle*). WNK1 was also detected with immunoprecipitates of SPAK and OSR1 from HEK293 cells or MDCK cells, indicating that these form an endogenous complex in living cells (Fig. 1, *left* and *right*).

SPAK and OSR1 bind to the cation-chloride transporters KCC3, NKCC1, and NKCC2 through a putative binding motif (R/K)FX(V/I) within the N-terminal tails of the transporters (22). In a yeast two-hybrid screen, SPAK was found to bind to WNK4, which contains a putative binding motif (23). A search of the amino acid sequences of human WNK1 revealed the presence of four putative SPAK-binding motifs (Fig. 2*A*). To further investigate the role of these motifs in WNK1 binding to STE20-related kinases, we co-expressed various forms of WNK1 with SPAK or OSR1 and performed co-immunoprecipitation experiments. Wild-type WNK1 was found to bind strongly to rat SPAK and mouse OSR1. WNK1(F1258A/F1869A) or WNK1(F1946A/F1958A), in which we mutated two of four SPAK-binding motifs by replacing the Phe residues with Ala, moderately decreased binding to SPAK/OSR1, and the additional mutations to the binding motifs of WNK1 showed gradually weak binding to SPAK/OSR1 depending on the number of mutations (Fig. 2*B*). These results suggested that WNK1 can associate with SPAK/OSR1 through four putative binding motifs.

WNK1 Phosphorylates the Evolutionary Conserved Serine Residues of SPAK and OSR1—To achieve specific and efficient phosphorylation of their substrates, many Ser/Thr protein kinases interact with the substrate via sites distinct from the phosphoacceptor sequence (28, 29). We first investigated whether SPAK and OSR1 are substrates of WNK1 kinase. By expression in bacteria, we produced a GST-tagged rat SPAK(KM) in which the Lys residue within subdomain II was replaced with Met. FLAG-tagged WNK1 was isolated from HEK293 cells and added to GST-SPAK(KM), and the mixture was analyzed by an *in vitro* kinase assay in the presence of [γ-^{32}P]ATP. In addition to WNK1 autophosphorylation, we observed that SPAK(KM) was phosphorylated in a time-dependent manner (Fig. 3*A*, *Wild type*). This phosphorylation was dependent on the kinase activity of WNK1 since phosphorylation was barely detectable when a kinase-dead form of WNK1 was used (Fig. 3*A*, *D368A*). To prove that SPAK is directly phosphorylated by WNK1 and not by putative kinases complexed with WNK1, we isolated several bacterially expressed WNK1 fragments tagged with GST. *In vitro* kinase analysis showed that the purified wild-type WNK1-(1–665) directly phosphorylated SPAK, whereas three forms of kinase-dead WNK1, K233M, D368A, or S382A, did not (Fig. 3*B*). Thus, our results indicated that the STE20-like kinase SPAK is a direct substrate of WNK1.

We next performed *in vitro* kinase assays using several deletion mutants of SPAK (Fig. 4*A*). GST-SPAK-(348–553) and GST-SPAK-(369–553), but not GST-SPAK-(400–553), were phosphorylated by WNK1, indicating that the WNK1 phosphorylation site(s) is located in the C-terminal regulatory region (369–400) of SPAK (Fig. 4*B*). Full-length GST-SPAK and GST-SPAK-(1–399) were also phosphorylated by WNK1, but the phosphorylation of these proteins is weaker than that of the C-terminal regulatory domain alone (Fig. 4*B*). It seems likely that the WNK1 phosphorylation site of SPAK is covered by the N-terminal region of SPAK including the kinase domain. There are four Ser/Thr residues, Ser-379, Ser-380, Thr-386, and Ser-394, within the 369–400 fragment of SPAK (Fig. 4*C*). To determine which residues are the site(s) of phosphorylation, various SPAK mutants were tested as substrates.

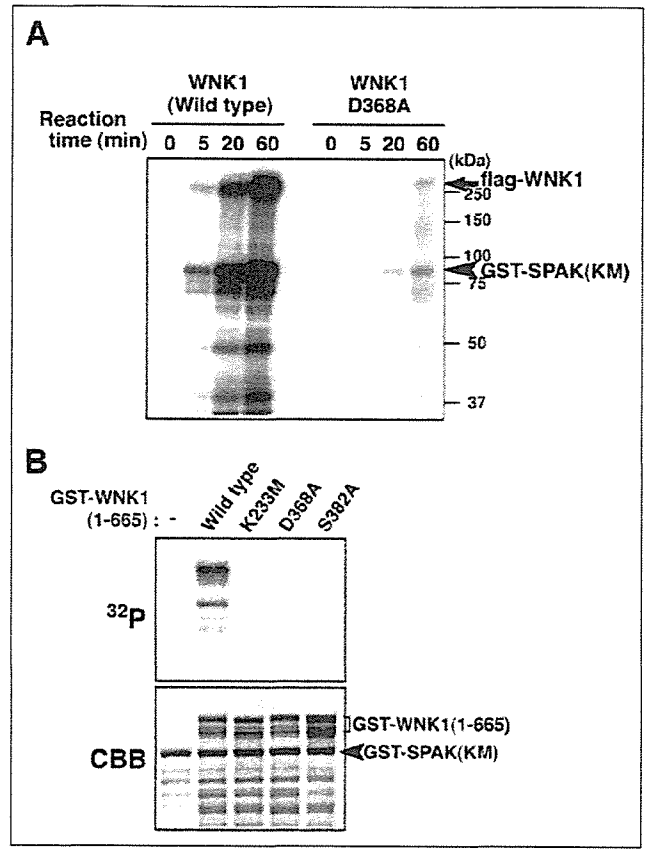

FIGURE 3. **WNK1 directly phosphorylates SPAK protein.** *A*, wild-type WNK1, but not kinase-dead WNK1 (WNK1(D368A)), mediates phosphorylation of SPAK. FLAG-tagged WNK1 and WNK1(D368A) isolated from transfected HEK293 cells were mixed with a GST-tagged kinase-dead form of SPAK (SPAK(KM)) and subjected to an *in vitro* kinase assay. The reaction was stopped at the indicated time points by the addition of SDS sample buffer. The protein complexes were separated by SDS-PAGE, and phosphorylated proteins were visualized by an image analyzer (BAS 2500). *B*, several bacterially produced GST-WNK1 fragments (wild type and three kinase-dead mutants (K233M, D368A and S382A)) and GST-SPAK(KM) were subjected to an *in vitro* kinase assay as indicated. Proteins were separated by SDS-PAGE and then visualized by Coomassie Brilliant Blue staining (*CBB*) and image analyzer (^{32}*P*).

The fragment 348–553(S380A) was not phosphorylated, indicating that Ser-380 is a major site of WNK1 phosphorylation (Fig. 4*B*). MS/MS analysis of tryptic peptides generated from phosphorylated recombinant SPAK proteins also indicated that Ser-380 is the site of phosphorylation (data not shown). Two small conserved regions were found in the C-terminal regions of SPAK and OSR1 and were named the PF1 and PF2 domains, respectively (Fig. 4*A*). Ser-380 of rat SPAK is located within the PF1 domain, and this Ser residue was highly conserved in other SPAK-related kinases, OSR1 and *Drosophila* Fray (Fig. 4*C*). We mutated the equivalent serine residue (Ser-325) in OSR1 to an Ala residue and examined phosphorylation by the WNK kinases. We found that both FLAG-WNK1 and FLAG-WNK4 were able to phosphorylate the full-length kinase-dead forms of SPAK and OSR1 but that mutation of the Ser residues to Ala of SPAK and OSR1 completely abolished or significantly reduced the phosphorylation (Fig. 4*D*). These data suggested that WNK1 phosphorylates these specific serine residues in SPAK-related kinases.

Ser-325 mutation of OSR1 Causes Its Activation—To examine the role that Ser phosphorylation of SPAK-related kinases plays in their regulation, we generated several mutants of OSR1. It has been recently reported that the N-terminal regulatory domain of p21-activated pro-

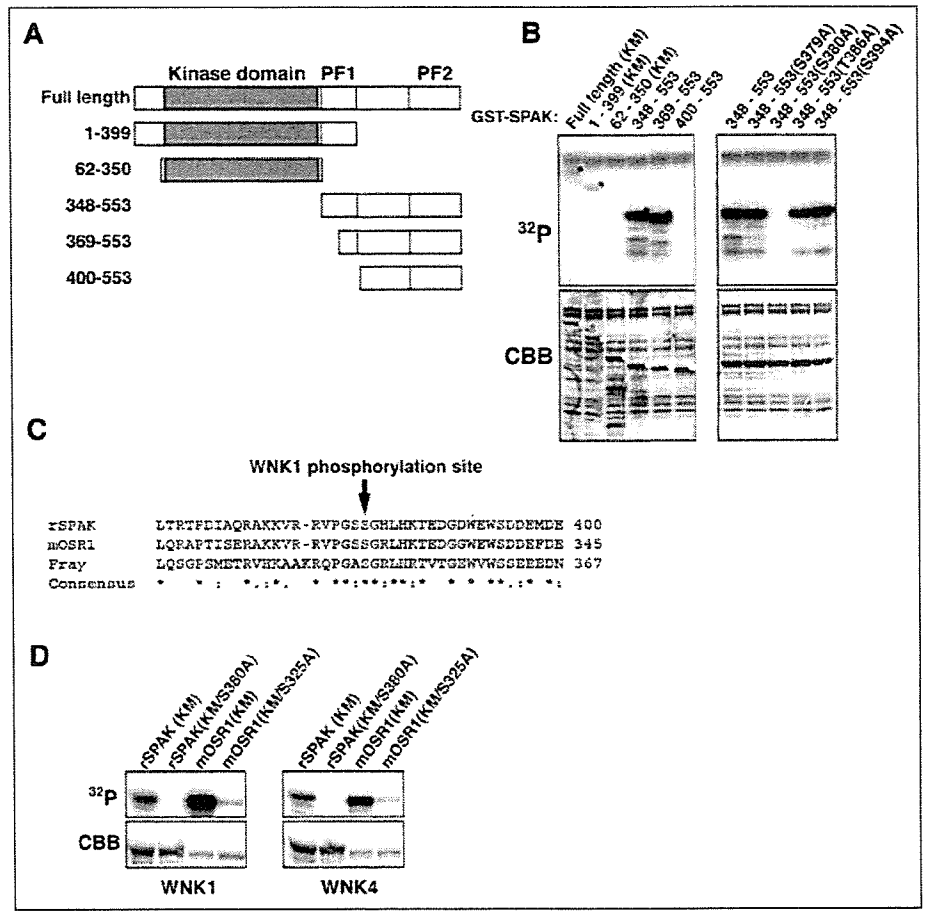

FIGURE 4. **WNK1 phosphorylates the conserved Ser residue in SPAK and OSR1.** *A*, schematic diagram of rat SPAK. Conserved domains among the SPAK-type STE20-related kinases are indicated as follows: kinase domain, PF1 domain (*PF1*), and PF2 domain (*PF2*). Fragments used in this study are also shown. *B*, GST-WNK1-(1–665) *in vitro* kinase assays were performed using the indicated GST-SPAK proteins as substrates and analyzed as in Fig. 3*B*. *Asterisks* indicate the sizes of the substrates. *CBB*, Coomassie Brilliant Blue staining. *C*, the amino acid sequence around the phosphorylation site of rat SPAK (*rSPAK*) is compared with that of mouse OSR1 (*mOSR1*) and *Drosophila* Fray by the ClustalW program. *Asterisks*, identical amino acids; *single* and *double dots*, weakly and strongly similar amino acids, respectively, determined by the criteria of the ClustalW program. *D*, FLAG-WNK1 (*left*) and FLAG-WNK4 (*right*) were isolated from transfected HEK293 cells and subjected to an *in vitro* kinase assay. GST fusion proteins of kinase-inactive SPAK(KM) or OSR1(KM) with or without the Ser to Ala point mutation were used as substrates and analyzed as in *panel B*.

tein kinase (PAK) is a physiological substrate of OSR1 (30). Wild-type GST-OSR1 exhibited a small amount of autophosphorylation, detectable by long exposure of the gel, but GST-OSR1KM showed no detectable activity (Fig. 5*A*). Since mutation of OSR1 Ser-325 to Asp mimics phosphorylation of this site, we generated GST-OSR1(S325D) and tested its activity. GST-OSR1(S325D) showed increased phosphorylation of GST-PAK3-(65–136), relative to wild-type OSR1 (Fig. 5*B*), indicating that the mutation Ser-325 to Asp of OSR1 causes constitutively activation of OSR1. Surprisingly, the mutation of the same site to Ala or Gly, which was expected to abolish phosphorylation, also resulted in causing constitutively activation of OSR1 (Fig. 5*B*, GST-OSR1(S325A), and data not shown). To further investigate the mechanisms of OSR1 activation, we examined several truncated forms of OSR1 (Fig. 5*C*). OSR1-(1–433) and OSR1-(1–344), truncated proteins lacking the PF2 domain, exhibited higher kinase activities than wild-type OSR1. In contrast, OSR1-(1–300), a truncated protein lacking both the PF1 and the PF2 domains, showed no detectable kinase activity (Fig. 5*D*). These results suggested that the PF1 domain of OSR1 is essential for kinase catalytic activity and that the PF2 domain is involved in regulating the catalytic activity.

SPAK and OSR1 Directly Phosphorylate the N-terminal Tail of Cation-Chloride Cotransporters—The activity of NKCC1 is regulated by phosphorylation/dephosphorylation, and examination of phosphorylation sites on NKCC1 revealed that three Thr residues in the N-terminal region, Thr-184, Thr-189, and Thr-202, are necessary for transport activity (19). NKCC2 and NCC are also members of the family of cation-chloride-coupled cotransporters, and the N-terminal regions of both cotransporters are conserved with that of NKCC1 (Fig. 6*A*). To test the possibility that SPAK and OSR1 are responsible for the phosphorylation of NKCC1, and also regulate NKCC2 and NCC, we prepared GST-tagged N-terminal fragments of each of these transporters. Both FLAG-SPAK and FLAG-OSR1 isolated from HEK293 cells were found to phosphorylate GST-NKCC2-(1–181), NKCC1-(1–289) and NCC-(1–138) (Fig. 6*B*). These proteins were also phosphorylated by GST-OSR1(S325D) *in vitro* (Fig. 6*C*), suggesting that phosphorylation was direct. The intensity of each phosphorylated band is comparable with or much higher than that observed using the GST-PAK3-(65–136) substrate, indicating that these cotransporters are good substrates for SPAK and OSR1. We next investigated the phosphorylation site(s) in the thiazide-sensitive transporter NCC using a series of mutations of the Ser/Thr residues that correspond to Thr-184, Thr-189, and Thr-202 of NKCC1. The T53A, T58A, and S71A mutants of NCC showed slightly reduced phosphorylation when compared with wild-type NCC. Moreover, there was no detectable increase in phosphorylation of the triple mutant, T53A/T58A/S71A (Fig. 6*D*). These results suggested that at least *in vitro*, SPAK/OSR1 directly phosphorylates the conserved Ser/Thr residues within the N-terminal regulatory region of NCC corresponding to shark NKCC1.

WNK1 and SPAK/OSR1 Are Activated by Low Cl^- Hypotonic Stress—Recent reports have shown that activation of shark and human Na-K-Cl cotransporter (NKCC1) by low Cl^- hypotonic stimulation is inhibited in cells expressing a dominant-negative mutant of SPAK and that the phosphorylation state of NKCC1 correlates with that of SPAK (24). Therefore, we tested whether hypotonic and low Cl^- conditions in cells

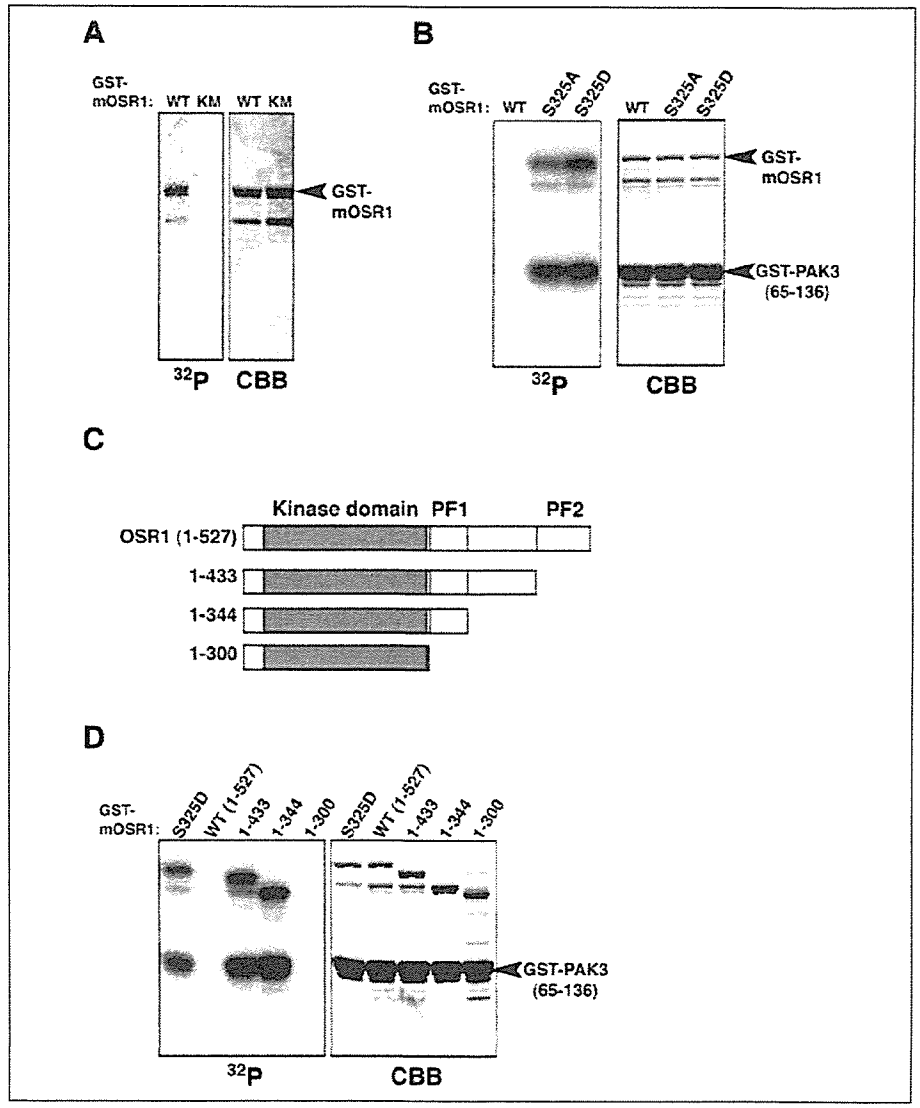

FIGURE 5. **Effects of WNK1 phosphorylation site modification on OSR1 activity *in vitro*.** *A*, kinase assays were performed with equal amounts of GST-tagged wild-type SPAK (*WT*) and kinase-dead form of OSR1(KM). *mOSR1*, mouse OSR1. *B*, GST-OSR1, GST-OSR1(S325A), and GST-OSR1(S325D) proteins were examined for their kinase activity toward GST-PAK3-(65–136). *C*, schematic diagram of mouse OSR1. Fragments used in *panel D* are also shown. *D*, the kinase activities of several OSR1 mutants were measured by *in vitro* kinase assay using GST-PAK3-(65–136) as a substrate. *CBB*, Coomassie Brilliant Blue staining.

lead to the activation of SPAK/OSR1. HEK293 cells were incubated with isotonic or low Cl^- hypotonic buffer, and endogenous WNK1 was immunoprecipitated and subjected to *in vitro* kinase assay using GST-SPAK-(348–553) as a substrate. We found that WNK1 kinase activity increased within 5 min and was sustained for at least 60 min by incubation in low Cl^- hypotonic conditions (Fig. 7*A*). We next examined the effect of low Cl^- hypotonic stimulation on phosphorylation and activation of SPAK/OSR1. When HEK293 cells transfected with an empty vector were incubated with hypotonic and low Cl buffer, SPAK/OSR1 autophosphorylation and kinase activity against GST-PAK3-(65–136) were increased (Fig. 7*B*). The phosphorylation of Ser-325 in OSR1 also occurred in cells under hypotonic and low Cl conditions. These results, together with those obtained *in vitro*, suggested that WNK1 functions as an activator for SPAK/OSR1 in response to Cl hypotonic stress in cells.

To clarify the role of the WNK/SPAK/OSR1 pathway in the phosphorylation of NCC, we performed a ^{32}P labeling experiment. Because we were unable to detect endogenous NCC in HEK293 cells or other cell lines by immunoblotting and immunostaining, T7-tagged mouse NCC was expressed in HEK293 cells. As shown in Fig. 7*C*, NCC was highly phosphorylated under low Cl^- hypotonic conditions. This result agreed well with the *in vitro* phosphorylation data and suggested that activation of the WNK1/SPAK/OSR1 pathway leads to the enhanced phosphorylation of NCC in cells.

DISCUSSION

In this study, we identified the STE20-like kinases, SPAK and OSR1, as targets of WNK1. WNK1 phosphorylates SPAK/OSR1 at a Ser residue within the PF1 domain, which is highly conserved among the mammalian SPAK/OSR1, *Drosophila* Fray, and *Caenorhabditis elegans* Y59A8B.23 gene products. WNK4 and WNK3 were also able to phosphorylate this residue (Fig. 2*F* and data not shown). In addition, *C. elegans* WNK1 phosphorylated the conserved Ser residue of the *C. elegans* SPAK/OSR1 homolog *in vitro*.[3] Thus, phosphorylation of SPAK/OSR1 by WNK kinase may be a common regulatory mechanism among species.

OSR1 mutants having point mutants in their PF1 domain or trunca-

[3] T. Moriguchi and H. Shibuya, unpublished data.

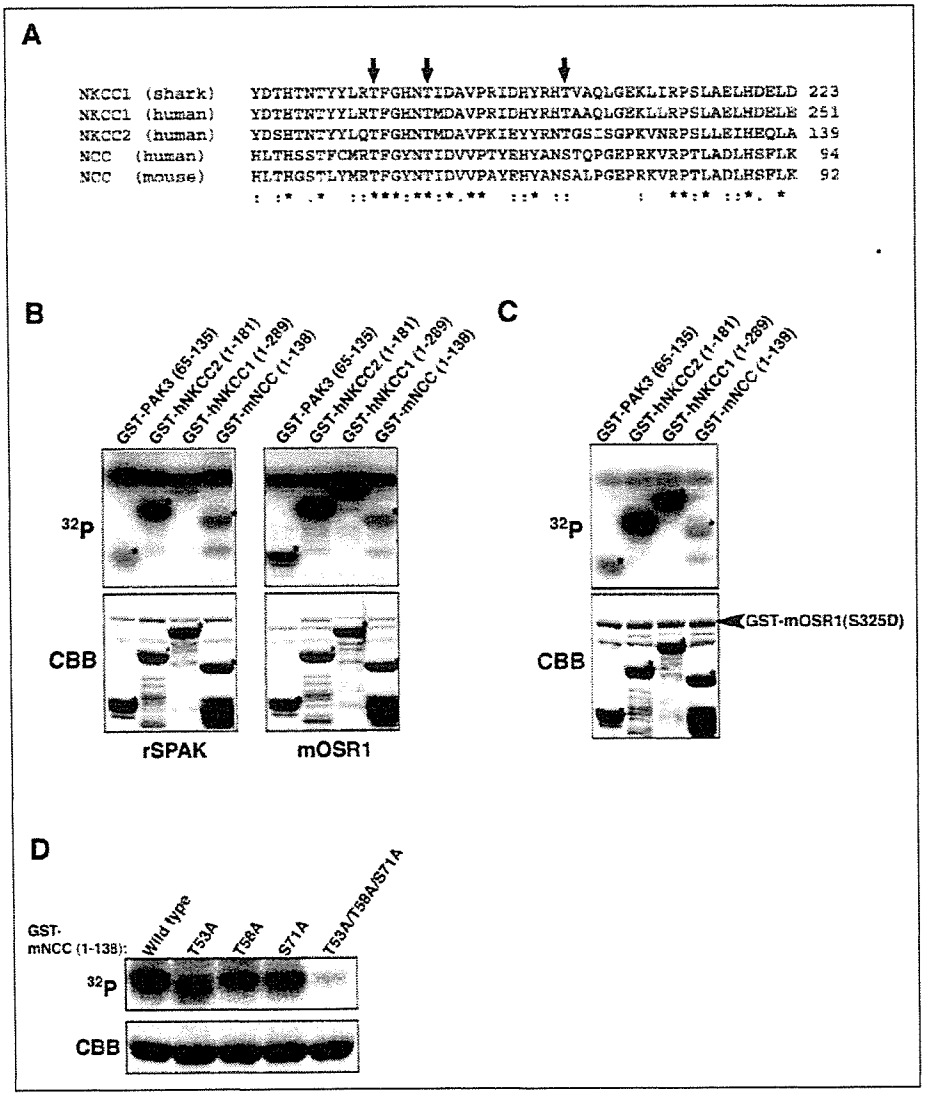

FIGURE 6. **N-terminal regulatory tail of cation-chloride-coupled cotransporter is phosphorylated by SPAK and OSR1.** *A*, alignment of the amino acid sequences of the regulatory regions in the N terminus of cation-chloride-coupled cotransporter, shark NKCC1, human NKCC1, human NKCC2, human NCC, and mouse NCC (*mNCC*). *Asterisks*, identical amino acids; *single* and *double dots*, weakly and strongly similar amino acids, respectively, were determined by the criteria of ClustalW program. *B*, T7-SAPK (*left*) or T7-OSR1 (*right*) isolated from HEK293 cells were assayed with GST-PAK3-(65–136), GST-hNKCC2-(1–181), GST-hNKCC1-(1–289), and GST-mNCC-(1–138) as substrates. Proteins were separated by SDS-PAGE and visualized by Coomassie Brilliant Blue (*CBB*) staining and an image analyzer (BAS 2500). *Asterisks* indicate the sizes of the substrates. *mOSR1*, mouse OSR1. *C*, GST-OSR1(S325D) was assayed for kinase activity as in *panel B*. *D*, GST-fusion proteins of NCC N-terminal fragments with the indicated Ser/Thr to Ala point mutations were used as substrates in GST-OSR1(S325D) kinase assays and analyzed as in *panel B*.

tion mutants lacking the PF2 domain exhibited higher kinase activities than wild-type OSR1 (Fig. 5). Moreover, a truncated mutant lacking the PF1 domain of OSR1 displayed no detectable kinase activity (Fig. 5*D*). It has been reported that many STE20-related kinases contain autoinhibitory domains and that removal of these regulatory domains results in a significant increase in kinase activity (31). Therefore, our results suggested that mutation of Ser-325 may cause constitutive activation of kinase activity due to conformational changes resulting from removal of the autoinhibitory PF2 domain rather than by an effect of negative charge. In the case of OSR1, the PF1 domain appeared to play an essential role in kinase catalytic activity, whereas the PF2 domain might be involved in regulating catalytic activity.

Mutation of the site in OSR1 that is phosphorylated by WNK1 resulted in enhanced OSR1 kinase activity, indicating that WNK1 plays an important role in the activation of SPAK and OSR1. However, *in vitro* phosphorylation of recombinant SPAK and OSR1 proteins by WNK1 or co-expression of SPAK and OSR1 with WNK1 in cells resulted in only weak activation of SPAK and OSR1 (data not shown). Therefore, WNK1 might not be the sole activator of SPAK and OSR1. The phosphorylation of multiple sites by several kinases has been shown to be required for the full activation of some kinases. For example, Akt is activated by phosphorylation on two residues, one in the activation loop of the kinase domain and the other located C-terminal to the catalytic domain (32). Phosphorylation of these sites in Akt is catalyzed by two kinases, 3-phosphoinositide-dependent kinase-1 (PDK1) and another tentatively called PDK2. Further studies will be needed to fully identify the kinase(s) that phosphorylates and activates SPAK/OSR1.

We also demonstrated that SPAK and OSR1 directly phosphorylate not only NKCC1 but also NKCC2 and NCC. These cation-chloride-cotransporters contain 12 transmembrane domains that are flanked by hydrophilic N- and C-terminal domains. It has been previously shown that three phosphorylation sites on the N terminus of shark NKCC1, Thr-189, Thr-184, and Thr-202, are necessary for full activation of transport activity (19). The sites of OSR1 phosphorylation in NCC include the three conserved Thr residues within the N-terminal regulatory region of the cation-chloride-coupled cotransporter family (Fig. 5), suggesting that WNK1 and SPAK/OSR1 could contribute to the regulation of transport activity. In fact, this hypothesis is supported by the recent finding that expression of both SPAK and WNK4 with NKCC1 in *Xenopus* oocytes results in a significant increase in NKCC1 activity (33). NCC, the mammalian thiazide-sensitive Na-Cl transporter, is expressed at the apical membrane of the distal convoluted

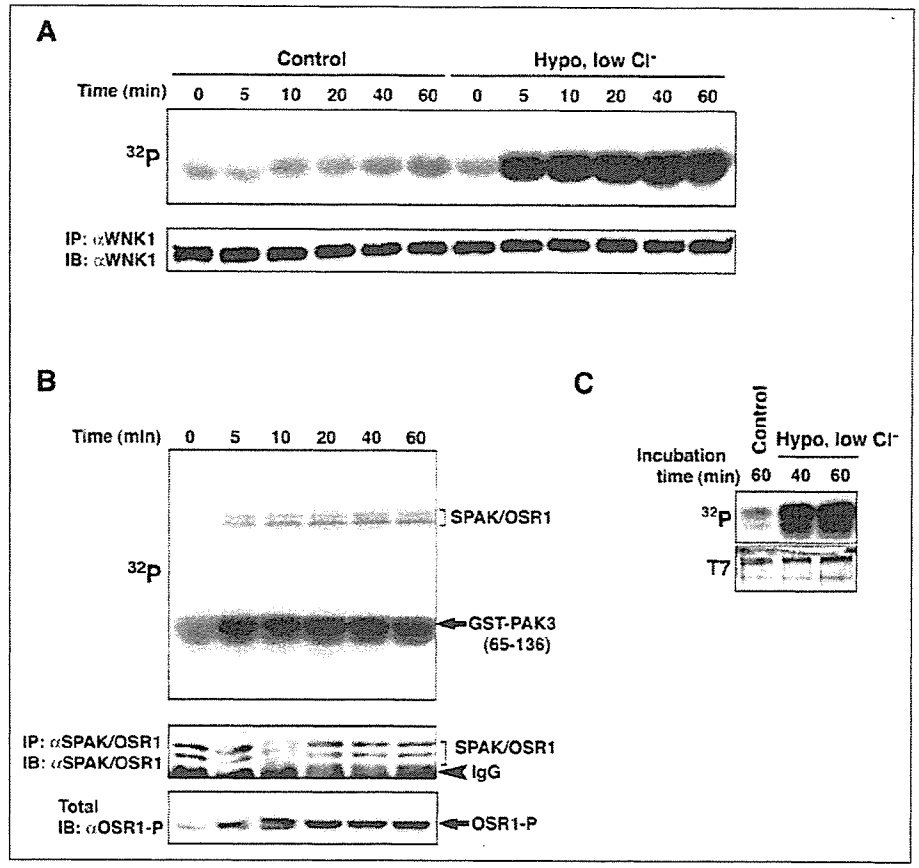

FIGURE 7. **Activation of WNK1 and SPAK/OSR1 by low Cl^- hypotonic stress.** *A*, HEK293 cells were incubated in isotonic buffer (*Control*) or low Cl^- hypotonic buffer (*Hypo, low Cl^-*) for the indicated times. The kinase activity of endogenous WNK1 was measured by an immune complex kinase assay using GST-SPAK-(348–553) as a substrate. The amount of immunoprecipitated WNK1 was detected by immunoblotting with the WNK1 antibody (immunoprecipitation (*IP*), αWNK1; immunoblotting (*IB*), αWNK1), and the phosphorylated GST-SPAK-(348–553) was detected by an image analyzer (BAS 2500) (^{32}P). *B*, HEK293 cells were incubated in low Cl^- hypotonic buffer for the indicated times. Endogenous SPAK/OSR1 was immunoprecipitated with the SPAK/OSR1 antibody, and subjected to an immune complex kinase assay using GST-PAK3-(65–136) as a substrate. The amount of SPAK/OSR1 in each immune complex was determined by immunoblotting (immunoprecipitation, αSPAK/OSR1; immunoblotting, αSPAK/OSR1). To monitor the Ser phosphorylation state of OSR1, lysates prepared from transfected cells were subjected to immunoblotting with the phospho-OSR1 antibody. Similar results were obtained in three different experiments. *C*, phosphorylation of T7-tagged NCC in HEK293cells. HEK293 cells were transfected with T7-NCC, metabolically labeled with [^{32}P]phosphate for 6 h, and then placed with isotonic buffer (*Control*) or low Cl hypotonic buffer for the indicated times prior to lysing. T7-NCC was immunoprecipitated using αT7 antibody.

tubule. Loss-of-function mutations in NCC have been shown to cause Gitelman syndrome, a disease characterized by salt wasting, hypokalemic metabolic alkalosis, and hypocalciuria. These clinical symptoms are the opposite of the symptoms observed in PHA II patients. The mutations in WNK1 associated with PHA II are intron deletions that cause increased expression of WNK1. Our findings supported the hypothesis that WNK1 phosphorylates and activates NCC, and this may provide a good explanation for pathogenesis of PHA II. However, the physiological relevance of these phosphorylation events to hypertension must be further evaluated by examining the regulation of NCC transport activity. In contrast to NCC, NKCC2, the bumetanide-sensitive cotransporter, is expressed in the apical membrane of the thick ascending limb of Henle's loop. Disruption of the *NKCC2* gene causes Bartter syndrome, an autosomal recessive disease characterized by metabolic alkalosis, hypokalemia, and hypercalciuria accompanied by a reduction in arterial blood pressure. Thus, it might be possible that activation of NKCC2 could account for hyperkalemia and hypertension in patients harboring *WNK1* mutations.

Tissue distribution reveals that WNK1 is widely expressed (1, 2). *WNK1*-deficient mice exhibit embryonic lethality, which indicates that WNK1 has important functions in many tissues, in addition to the kidney (34). NKCC1, SPAK, and OSR1 are also ubiquitously expressed and have multiple functions, such as regulation of cell volume, modulation of neuron excitability, AP-1-dependent gene expression, and regulation of the actin cytoskeleton (17, 30, 35). In this study, we identified a signaling pathway consisting of the PHA II disease-associated kinase WNK1 and the STE20-related kinases SPAK and OSR1, which culminates in the phosphorylation of several cotransporters. We hope that these findings will contribute to our understanding of the biological function for WNK1, not only in the pathogenesis of hypertension but also in other processes.

Acknowledgments—We thank T. Suganami and Y. Ogawa for valuable discussions, T. Akiyama for reagents, M. Lamphier for critical reading of the manuscript, and K. Nakamura and S. Tobiume for technical assistance.

Addendum—While this report was in preparation, a study describing WNK1/WNK4 phosphorylation of the same key serine residue, but also identifying an additional threonine residue within the activation loop, was published (36).

REFERENCES

1. Xu, B., English, J. M., Wilsbacher, J. L., Stippec, S., Goldsmith, E. J., and Cobb, M. H. (2000) *J. Biol. Chem.* **275**, 16795–16801
2. Verissimo, F., and Jordan, P. (2001) *Oncogene* **20**, 5562–5569
3. Min, X., Lee, B. H., Cobb, M. H., and Goldsmith, E. J. (2004) *Structure (Camb.)* **12**, 1303–1311
4. Wilson, F. H., Disse-Nicodeme, S., Choate, K. A., Ishikawa, K., Nelson-Williams, C., Desitter, I., Gunel, M., Milford, D. V., Lipkin, G. W., Achard, J. M., Feely, M. P., Dussol, B., Berland, Y., Unwin, R. J., Mayan, H., Simon, D. B., Farfel, Z., Jeunemaitre, X., and Lifton, R. P. (2001) *Science* **293**, 1107–1112
5. Wilson, F. H., Kahle, K. T., Sabath, E., Lalioti, M. D., Rapson, A. K., Hoover, R. S., Hebert, S. C., Gamba, G., and Lifton, R. P. (2003) *Proc. Natl. Acad. Sci. U. S. A.* **100**, 680–684
6. Yang, C. L., Angell, J., Mitchell, R., and Ellison, D. H. (2003) *J. Clin. Investig.* **111**, 1039–1045
7. Yang, S. S., Yamauchi, K., Rai, T., Hiyama, A., Sohara, E., Suzuki, T., Itoh, T., Suda, S., Sasaki, S., and Uchida, S. (2005) *Biochem. Biophys. Res. Commun.* **330**, 410–414
8. Kahle, K. T., Wilson, F. H., Leng, Q., Lalioti, M. D., O'Connell, A. D., Dong, K., Rapson, A. K., MacGregor, G. G., Giebisch, G., Hebert, S. C., and Lifton, R. P. (2003) *Nat. Genet.* **35**, 372–376
9. Kahle, K. T., Gimenez, I., Hassan, H., Wilson, F. H., Wong, R. D., Forbush, B., Aron-

son, P. S., and Lifton, R. P. (2004) *Proc. Natl. Acad. Sci. U. S. A.* **101,** 2064–2069
10. Kahle, K. T., Macgregor, G. G., Wilson, F. H., Van Hoek, A. N., Brown, D., Ardito, T., Kashgarian, M., Giebisch, G., Hebert, S. C., Boulpaep, E. L., and Lifton, R. P. (2004) *Proc. Natl. Acad. Sci. U. S. A.* **101,** 14877–14882
11. Yamauchi, K., Rai, T., Kobayashi, K., Sohara, E., Suzuki, T., Itoh, T., Suda, S., Hayama, A., Sasaki, S., and Uchida, S. (2004) *Proc. Natl. Acad. Sci. U. S. A.* **101,** 4690–4694
12. Lee, B. H., Min, X., Heise, C. J., Xu, B. E., Chen, S., Shu, H., Luby-Phelps, K., Goldsmith, E. J., and Cobb, M. H. (2004) *Mol. Cell* **15,** 741–751
13. Xu, B. E., Stippec, S., Lenertz, L., Lee, B. H., Zhang, W., Lee, Y. K., and Cobb, M. H. (2004) *J. Biol. Chem.* **279,** 7826–7831
14. Xu, B. E., Stippec, S., Chu, P. Y., Lazrak, A., Li, X. J., Lee, B. H., English, J. M., Ortega, B., Huang, C. L., and Cobb, M. H. (2005) *Proc. Natl. Acad. Sci. U. S. A.* **102,** 10315–10320
15. Xu, B. E., Stippec, S., Lazrak, A., Huang, C. L., and Cobb, M. H. (2005) *J. Biol. Chem.* **280,** 34218–34223
16. Hebert, S. C., Mount, D. B., and Gamba, G. (2004) *Pfluegers Arch. Eur. J. Physiol.* **447,** 580–593
17. Russell, J. M. (2000) *Physiol. Rev.* **80,** 211–276
18. Haas, M., and Forbush, B., III (2000) *Annu. Rev. Physiol.* **62,** 515–534
19. Darman, R. B., and Forbush, B. (2002) *J. Biol. Chem.* **277,** 37542–37550
20. Waldegger, S., Barth, P., Forrest, J. N., Jr., Greger, R., and Lang, F. (1998) *Pfluegers Arch. Eur. J. Physiol.* **436,** 575–580
21. Klein, J. D., Lamitina, S. T., and O'Neill, W. C. (1999) *Am. J. Physiol.* **277,** C425–C431
22. Piechotta, K., Lu, J., and Delpire, E. (2002) *J. Biol. Chem.* **277,** 50812–50819
23. Piechotta, K., Garbarini, N., England, R., and Delpire, E. (2003) *J. Biol. Chem.* **278,** 52848–52856
24. Dowd, B. F., and Forbush, B. (2003) *J. Biol. Chem.* **278,** 27347–27353
25. Okabe, T., Nakamura, T., Nishimura, Y. N., Kohu, K., Ohwada, S., Morishita, Y., and Akiyama, T. (2003) *J. Biol. Chem.* **278,** 9920–9927
26. James, P., Halladay, J., and Craig, E. A. (1996) *Genetics* **144,** 1425–1436
27. Natsume, T., Yamauchi, Y., Nakayama, H., Shinkawa, T., Yanagida, M., Takahashi, N., and Isobe, T. (2002) *Anal. Chem.* **74,** 4725–4733
28. Tanoue, T., Adachi, M., Moriguchi, T., and Nishida, E. (2000) *Nat. Cell Biol.* **2,** 110–116
29. Biondi, R. M., and Nebreda, A. R. (2003) *Biochem. J.* **372,** 1–13
30. Chen, W., Yazicioglu, M., and Cobb, M. H. (2004) *J. Biol. Chem.* **279,** 11129–11136
31. Dan, I., Watanabe, N. M., and Kusumi, A. (2001) *Trends Cell Biol.* **11,** 220–230
32. Brazil, D. P., Yang, Z. Z., and Hemmings, B. A. (2004) *Trends Biochem. Sci.* **29,** 233–242
33. Gagnon, K. B., England, R., and Delpire, E. (2005) *Am. J. Physiol.*, in press
34. Zambrowicz, B. P., Abuin, A., Ramirez-Solis, R., Richter, L. J., Piggott, J., Beltrandel-Rio, H., Buxton, E. C., Edwards, J., Finch, R. A., Friddle, C. J., Gupta, A., Hansen, G., Hu, Y., Huang, W., Jaing, C., Key, B. W., Jr., Kipp, P., Kohlhauff, B., Ma, Z. Q., Markesich, D., Payne, R., Potter, D. G., Qian, N., Shaw, J., Schrick, J., Shi, Z. Z., Sparks, M. J., Van Sligtenhorst, I., Vogel, P., Walke, W., Xu, N., Zhu, Q., Person, C., and Sands, A. T. (2003) *Proc. Natl. Acad. Sci. U. S. A.* **100,** 14109–14114
35. Li, Y., Hu, J., Vita, R., Sun, B., Tabata, H., and Altman, A. (2004) *EMBO J.* **23,** 1112–1122
36. Vitari, A. C., Deak, M., Morrice, N. A., and Alessi, D. R. (2005) *Biochem. J.* **391,** 17–24

Vol 437|27 October 2005|doi:10.1038/nature04106

nature

LETTERS

A heterodimeric complex that promotes the assembly of mammalian 20S proteasomes

Yuko Hirano[1], Klavs B. Hendil[2], Hideki Yashiroda[1], Shun-ichiro Iemura[3], Ryoichi Nagane[3], Yusaku Hioki[3], Tohru Natsume[3], Keiji Tanaka[1] & Shigeo Murata[1,4]

The 26S proteasome is a multisubunit protease responsible for regulated proteolysis in eukaryotic cells[1,2]. It comprises one catalytic 20S proteasome and two axially positioned 19S regulatory complexes[3]. The 20S proteasome is composed of 28 subunits arranged in a cylindrical particle as four heteroheptameric rings, $\alpha_{1-7}\beta_{1-7}\beta_{1-7}\alpha_{1-7}$ (refs 4, 5), but the mechanism responsible for the assembly of such a complex structure remains elusive. Here we report two chaperones, designated proteasome assembling chaperone-1 (PAC1) and PAC2, that are involved in the maturation of mammalian 20S proteasomes. PAC1 and PAC2 associate as heterodimers with proteasome precursors and are degraded after formation of the 20S proteasome is completed. Overexpression of PAC1 or PAC2 accelerates the formation of precursor proteasomes, whereas knockdown by short interfering RNA impairs it, resulting in poor maturation of 20S proteasomes. Furthermore, the PAC complex provides a scaffold for α-ring formation and keeps the α-rings competent for the subsequent formation of half-proteasomes. Thus, our results identify a mechanism for the correct assembly of 20S proteasomes.

It is presumed that assembly of 20S proteasomes starts by the spontaneous formation of α-rings[6–8]; however, the exact mechanism responsible for α-ring formation remains elusive. Seven β-subunits, some of which are in precursor forms, are arranged on the α-ring to form a complex named the 'half-proteasome', which consists of one α-ring, one β-ring and the chaperone protein Ump1. To complete maturation of the 20S proteasome, two half-proteasomes dimerize, the propeptides of β-subunits are removed and Ump1 is degraded[9–11]. This model is based mainly on studies in yeast. In mammals, POMP or Proteassemblin, a homologue of yeast Ump1 referred to here as human Ump1 (hUmp1), is also implicated in assembly of 20S proteasomes[12–14]. However, the biogenesis of 20S proteasomes remains largely elusive, especially in mammalian cells.

To identify proteins that interact with mammalian proteasomes, β1i subunits with a Flag tag were expressed in cells and anti-Flag immunoprecipitates were analysed by liquid chromatography coupled with tandem mass spectrometry[15]. We identified hUmp1 in addition to almost all of the subunits of 20S proteasomes and 19S regulatory complexes. We also identified two molecules with previously unknown relevance to proteasomes. One was Down syndrome critical region 2 (DSCR2), a small leucine-rich protein of 288 amino acids[16] that we have renamed PAC1. The other was a protein of 264 amino acids known as hepatocellular carcinoma associated gene 3 (HCCA3) (ref. 20), which we have renamed PAC2. Both PAC1 and PAC2 are ubiquitously expressed in mammals[17,20].

First, we confirmed that these molecules interact physically with proteasomes by transfecting Flag–PAC1 or Flag–PAC2 into HEK293T cells. The association increased on treatment of the cells with MG132, a proteasome inhibitor, in line with the increase in PAC1 and PAC2 expression (Supplementary Fig. 1a). Next, extracts of HeLa cells stably expressing Flag–PAC1 or Flag–PAC2 were fractionated by 8–32% glycerol gradient centrifugation. Both Flag–PAC1 and Flag–PAC2 were observed mainly in fractions containing sediments of precursor forms of proteasomes, as shown by the co-sedimentation of hUmp1, the unprocessed β1i (pro-β1i) subunit and α-subunits, and by the lack of chymotrypsin-like activity. Both Flag–PAC1 and Flag–PAC2 effectively co-precipitated with subunits from fraction 10 (Supplementary Fig. 1b, d). Moreover, even in fraction 16, which contained predominantly mature 20S proteasomes, they precipitated mainly with pro-β1i (Supplementary Fig. 1d), confirming that PAC1 and PAC2 associate specifically with precursor 20S proteasomes. Notably, the concentrations of precursor proteasomes were increased in both transfected cell lines (Supplementary Fig. 1c).

To examine the behaviour of endogenous PAC1 and PAC2 in detail, extracts from HEK293T cells were separated by lower density (4–24%) glycerol gradient centrifugation to resolve the precursor complexes. PAC1 and PAC2 were distributed mostly in the precursor fractions (Fig. 1a). Notably, the peaks of PAC1 and PAC2 were located in a fraction (fraction 12) lighter than that of the half-proteasomes (fraction 16), which contained hUmp1 and pro-β2. Moreover, the peaks of α5–α7 in precursor fractions were also located in fraction 12. Treatment with MG132 resulted in an accumulation of PAC1 and PAC2 in 20S proteasome fractions (Fig. 1a, right). The association of PAC1 and PAC2 with proteasomes was observed in fractions 12, 16 and 22 (Fig. 1b). When cells were treated with MG132, greater amounts of PAC1 and PAC2 were precipitated from fraction 22. Neither α4 nor α6 was associated with pro-β2 or hUmp1 in fraction 12. These results indicate that PAC1 and PAC2 form a complex with precursor 20S proteasomes before hUmp1 and the pro-β subunits are recruited, and suggest that PAC1 and PAC2 are chaperones for the maturation of 20S proteasomes and are released from or degraded by the newly assembled 20S proteasomes, analogous to the role of Ump1 in yeast[9–11].

To determine the composition of the peak of α-subunits that contained PAC1 and PAC2, fractions 12 and 16 were immunoprecipitated with antibodies against α6 and separated by two-dimensional polyacrylamide gel electrophoresis (2D-PAGE). Fraction 12 contained all seven α-subunits but no β-subunits, some of which were apparently detected in fraction 16 (Fig. 1c). Immunoblot analysis confirmed that all α-subunits except α1, which was difficult to distinguish by immunoblotting, were present in fraction 12 (Fig. 1d). The size of this complex (Fig. 1a), coupled with the absence of pro-β subunits or hUmp1 (Fig. 1a–c), means that it is

[1]Laboratory of Frontier Science, Core Technology and Research Center, Tokyo Metropolitan Institute of Medical Science, Bunkyo-ku, Tokyo 113-8613, Japan. [2]Institute of Molecular Biology and Physiology, University of Copenhagen, 13 Universitetsparken, DK 2100 Copenhagen, Denmark. [3]National Institute of Advanced Industrial Science and Technology, Biological Information Research Center, Koto-ku, Tokyo 135-0064, Japan. [4]PRESTO, Japan Science and Technology Agency, Kawaguchi, Saitama 332-0012, Japan.

most probably a ring of all seven α-subunits, namely an α-ring. Immunoprecipitation in lower salt conditions showed that PAC1 and PAC2 are near-stoichiometric components of α-rings and that the association of PAC1 and PAC2 with α-subunits is salt labile (Fig. 1e, f). PAC1 was detected at a wide range of isoelectric point (pI) values, suggesting that it undergoes posttranslational modification (Fig. 1f). These results suggest that the PAC1–PAC2 complex and hUmp1 are distinct entities that work at different points in 20S proteasome assembly, and that PAC1 and PAC2 function as chaperone-like molecules at an earlier stage of 20S proteasome assembly relative to hUmp1.

Next, we characterized the interaction between PAC1 and PAC2. Coexpression of PAC1 and PAC2 in *Escherichia coli* and *in vitro* cotranscription–translation (IVTT) indicated that the two proteins bind directly (Supplementary Fig. 2a, b). Furthermore, PAC1 tagged with glutathione *S*-transferase (GST) pulled down PAC2 tagged with haemagglutinin A (HA) but not HA–PAC1, whereas GST–PAC2 pulled down HA–PAC1 but not HA–PAC2 *in vitro* (Supplementary Fig. 2b), indicating that PAC1 and PAC2 form hetero-oligomers but not homo-oligomers. No direct interaction between the PAC complex and hUmp1 was detected (Supplementary Fig. 2c). To determine the stoichiometry of the PAC complex, we coexpressed 3× Flag–PAC1 and 6× His–PAC2 in *E. coli* and purified the complex. PAC1 and PAC2 formed a complex at 1:1 stoichiometry with a relative molecular mass (M_r) corresponding to bovine serum albumin (67,000; Fig. 2a, b), indicating that the complex is a heterodimer.

To clarify further the nature of the PAC complex, we examined the half-lives of PAC1 and PAC2 by pulse-chase experiments. Both PAC1 and PAC2 turned over rapidly with similar half-lives of about 40 min (Fig. 2c). Treating the cells with MG132 markedly prolonged their half-lives, indicating that the PAC heterodimer is degraded by proteasomes. Because assembly of 20S proteasomes is complete within 1 h (ref. 21), the half-life of the PAC complex is consistent with the complex functioning as a chaperone for proteasome assembly and with its degradation on the completion of 20S proteasomes assembly.

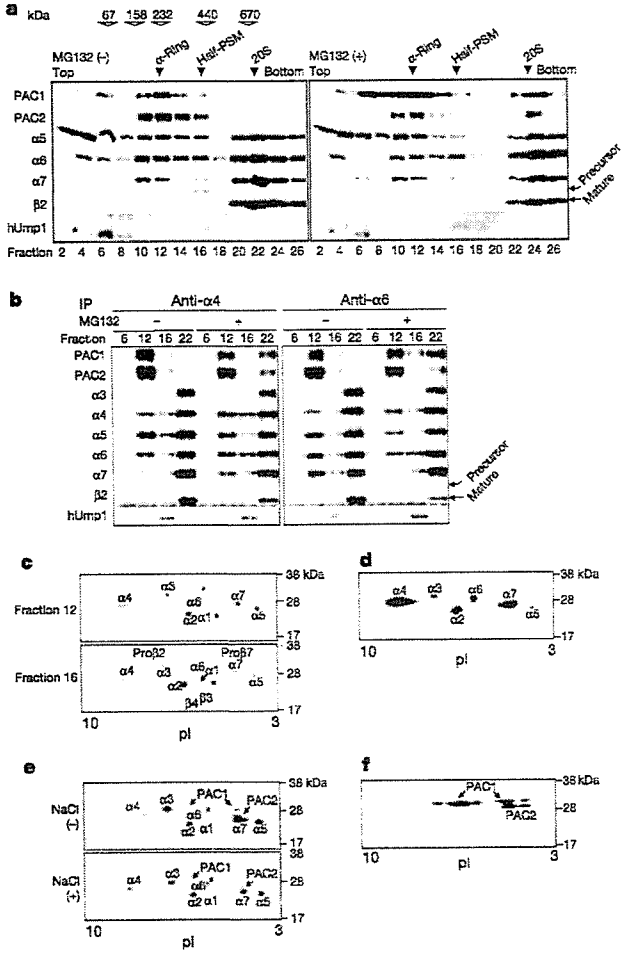

Figure 1 | PAC1 and PAC2 associate with precursor proteasomes. **a**, Glycerol gradient centrifugation (4–24%) of HEK293T cell extracts untreated or treated with MG132. Fractions were immunoblotted for the indicated proteins. Size markers and subcomplexes of proteasomes are indicated by open and filled arrowheads, respectively. Half-PSM indicates half-proteasomes. Asterisks indicate nonspecific bands. **b**, Fractions from **a** were immunoprecipitated with antibody against α4 or α6 and then subjected to immunoblotting. **c**–**f**, Fractions 12 (**c**–**f**) and 16 (**c**) from **a** were immunoprecipitated with beads conjugated to antibody against α6, washed with buffer A containing 150 mM (**c**, **d**), 0 mM or 50 mM (**e**, **f**) NaCl, eluted with glycine-HCl, and resolved by 2D-PAGE with silver (**c**) or Coomassie blue (**e**) staining. Asterisks denote unidentified spots. The top gel in **c** was immunoblotted with MCP231 and MCP34 antibodies against α-subunits and α4, respectively (**d**). The top gel in **e** was immunoblotted with antibodies against PAC1 and PAC2 (**f**). The non-uniformity of the spot intensity (**c**, **e**) may be due to a staining artefact because even in the half-proteasome fraction (fraction 16), which should contain all α-subunits in equal amounts, the spot intensities of α-subunits varied, resembling the pattern of fraction 12.

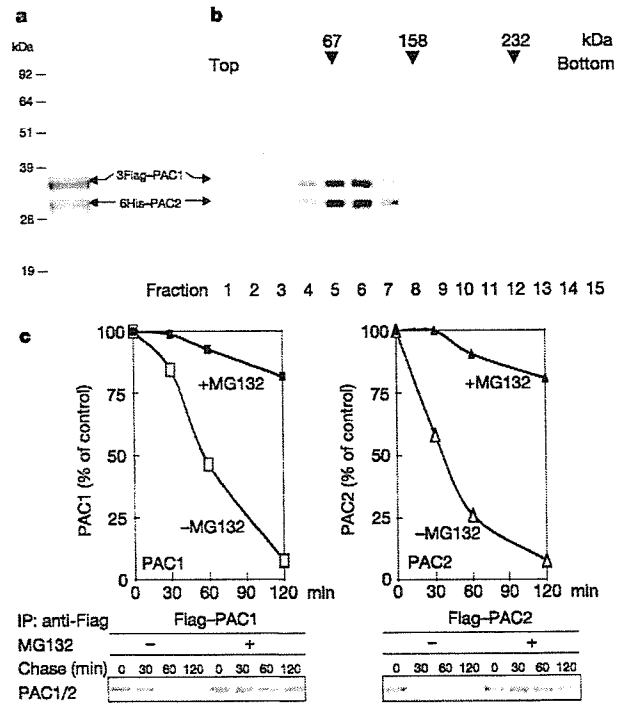

Figure 2 | The PAC1–PAC2 heterodimer is rapidly degraded by proteasomes. **a**, Coomassie blue staining of a copurified complex of 3× Flag–PAC1 and 6× His–PAC2 expressed in bacterial cells. **b**, The purified PAC complex in **a** was separated by 4–17% glycerol gradient centrifugation and subjected to SDS–PAGE with Coomassie staining. Arrowheads indicate size markers. **c**, Half-lives of PAC1 and PAC2. HeLa cells stably transfected with Flag–PAC1 or Flag–PAC2 were radiolabelled and chased in the presence or absence of MG132. Bottom panels show autoradiography; top panels show quantitative analysis of the bands.

To clarify the role of PAC1 and PAC2 in the assembly of the 20S proteasome *in vivo*, we used short interfering RNA (siRNA) to knock down the expression of PAC1 and PAC2. Knockdown of PAC1 resulted in loss of both PAC1 and PAC2 protein. Knockdown of PAC2 was also associated with a decrease in PAC1 protein (Fig. 3a), indicating that PAC1 and PAC2 are stable only when they form a heterodimer. Both PAC1- and PAC2-knockdown cells showed reduced proteolytic activity, as indicated by an assay of the antizyme-dependent degradation of ornithine decarboxylase (Supplementary Fig. 3a). Consequently, PAC-knockdown cells accumulated polyubiquitin-conjugated proteins, were sensitive to stress such as Cd^{2+}, and showed slow growth (Supplementary Fig. 3b–d).

We subjected the PAC-knockdown cells, as well as control and hUmp1-knockdown cells, to 4–24% glycerol gradient analysis. Notably, α-rings were hardly detected in either the PAC1- or the PAC2-knockdown cells (Fig. 3b). Instead, the α-subunits accumulated in fractions corresponding to half-proteasomes. This accumulation was not accompanied by an increase in pro-β2, pro-β5 or hUmp1, however, suggesting that the half-proteasomes were not normal. To confirm this notion, fraction 16 from the knockdown cells was immunoprecipitated with antibody against α6. Even though nearly equal amounts of α-subunits were loaded in the different samples, pro-β2, pro-β5 and hUmp1 were detected in much smaller amounts in PAC-knockdown cells (Fig. 3c), indicating that fraction 16 in PAC-knockdown cells contained mostly abnormally assembled α-subunits. This abnormal complex did not contain Rpt subunits, the components of 19S regulatory particles (Supplementary Fig. 3e, f), precluding the possibility that the mobility shift of α-subunits in PAC-knockdown cells was due to the premature association of α-subunits with Rpt subunits. On the basis of their sizes, these complexes are probably dimers of α-rings.

In hUmp1-knockdown cells, by contrast, we observed a marked reduction in 20S proteasomes but apparently normal α-rings and half-proteasomes, demonstrating the crucial role of hUmp1 in the dimerization of half-proteasomes. There was a strong increase in the free forms of some α-subunits in hUmp1-knockdown cells and a moderate increase in PAC-knockdown cells (Supplementary Fig. 3g). Assays of peptidase activities showed a significant reduction in activity of both the 20S and the 26S proteasome fractions in PAC-knockdown cells, although the effect of hUmp1 knockdown was more intense (Supplementary Fig. 3h). These data show definitively that the PAC complex has a pivotal role in the assembly of 20S proteasomes, specifically in keeping α-rings competent for the subsequent formation of half-proteasomes.

To elucidate the mechanism of PAC complex function, we tested the direct association of the complex with all of the subunits of 20S proteasomes. The PAC complex specifically interacted with α5 and α7, but not with other α-subunits or with any of the β-subunits *in vitro* (Supplementary Fig. 4a). Because Fig. 1a shows that the PAC1–PAC2 complex is found not only in α-ring fractions but also in lighter fractions, we considered whether it is involved in α-ring assembly. Immunoprecipitation with an antibody against Flag after the coexpression of all seven α-subunits, of which α5 was Flag-tagged, by IVTT showed that all α-subunits co-precipitated with Flag–α5 in larger amounts in the presence of the PAC complex than in its absence (Supplementary Fig. 4b). Immunoprecipitation with anti-Flag antibody after the coexpression of Flag–PAC1, PAC2 and α-subunits showed that PAC1 precipitated not only α5 and α7 but also all of the other α-subunits (Supplementary Fig. 4c), implying that it has a role in attracting α-subunits to each other.

We examined these interactions under more physiological conditions. Extracts of 293T cells that stably express Flag–PAC1 were separated by 4–24% glycerol gradient, and fractions corresponding to early α-subunit assembly intermediates and α-rings (fractions 8 and 12 in Fig. 1a, respectively) were immunoprecipitated with anti-Flag antibody and subjected to 2D-PAGE. PAC1 in fraction 12 co-precipitated all seven α-subunits, whereas PAC1 in fraction 8 co-precipitated several unidentified spots other than α-subunits, which made it difficult to identify α-subunits except for α5 and α7 by Coomassie staining (Fig. 4a, left). Immunoblot analysis showed that all α-subunits were present in the α-ring fraction, although α1 was difficult to distinguish (Fig. 4a, right), consistent with the findings in Fig. 1c. In contrast, PAC1 in fraction 8 co-precipitated a restricted set

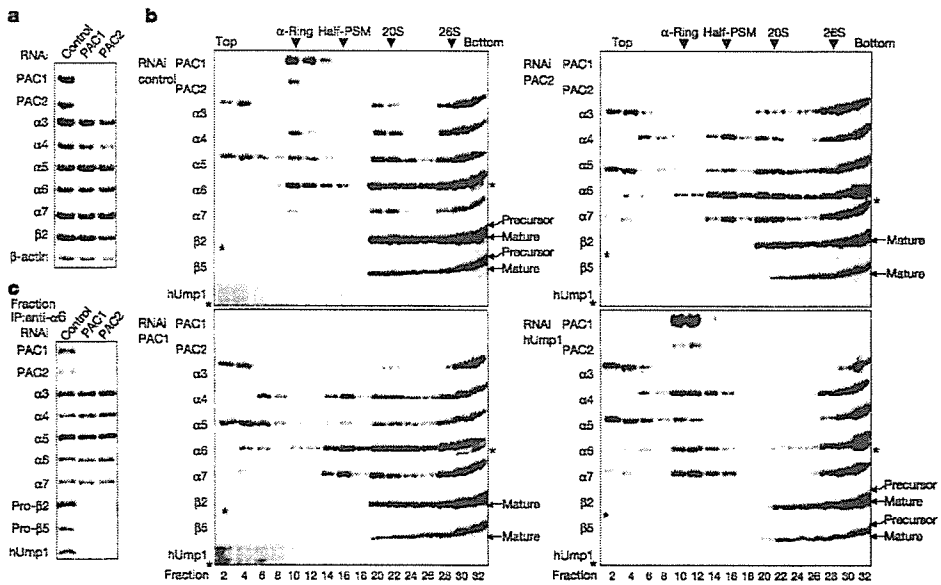

Figure 3 | siRNA-mediated knockdown of PAC1 and PAC2 impairs proteasome assembly. a–c, siRNA targeting PAC1 or PAC2, or control siRNA, was transfected into HEK293T cells. Knockdown of hUmp1 was also analysed in **b**. Whole-cell extracts (**a**), fractions separated by 4–24% glycerol gradient centrifugation (**b**), and immunoprecipitates obtained from fraction 16 in **b** with antibodies against α6 (**c**) were immunoblotted for the indicated proteins. Asterisks indicate nonspecific bands.

of α-subunits in which α3 and α4 were hardly detected. These results indicate that there is a hierarchy among α-subunits in their incorporation into α-rings, and that the PAC complex associates with the α-subunits before α-rings are complete, and functions as a scaffold for α-ring assembly.

Finally, we tested whether the complex of α-subunits in fraction 12 is a unique species. The affinity-purified complex from fraction 12 was subjected to native-PAGE. We found that the complex had a unique electrophoretic mobility (Fig. 4b). Moreover, the complex was eluted with a single sharp peak by anion-exchange chromatography (Fig. 4c). Thus, this complex is a unique species biochemically and is a genuine α-ring rather than a group of heterogeneous and incomplete α-ring precursors.

Our present work provides a model in which the chaperone complex PAC1–PAC2 mediates the formation of α-rings, keeps the rings competent for half-proteasome formation, and is required for proper proteasome maturation and cellular integrity (Fig. 4d). (See Supplementary Discussion for a more detailed description.)

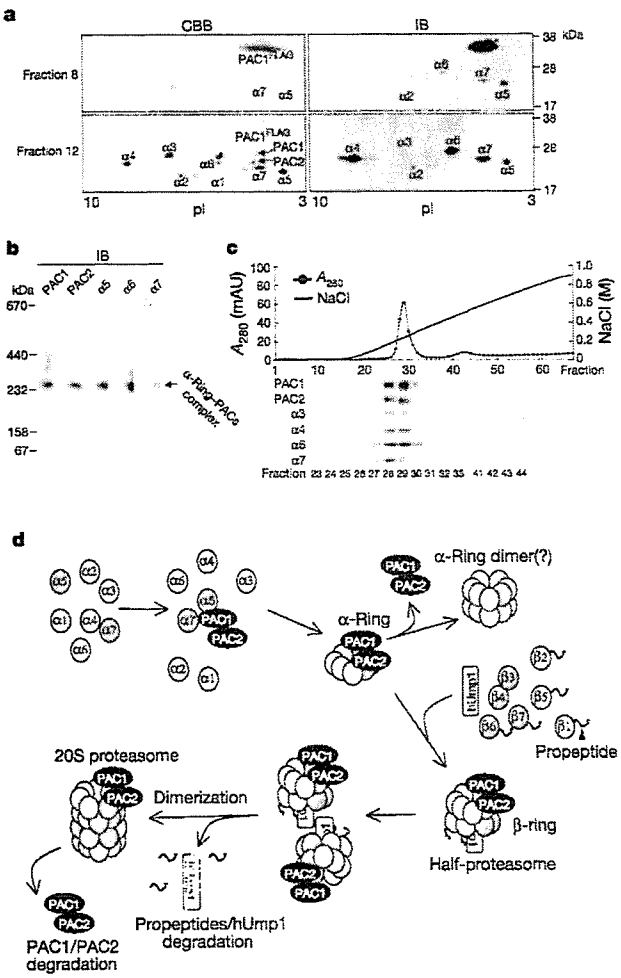

Figure 4 | PAC1–PAC2 provides a scaffold for α-ring formation. a, Extracts of HEK293T cells transfected with Flag–PAC1 were fractionated as in Fig. 1a. The Flag–PAC1 complexes from fractions 8 and 12 were purified with M2 agarose, resolved by 2D-PAGE and detected by Coomassie blue staining (left) or immunoblotting as in Fig. 1d (right). Asterisks denote unidentified spots. **b**, **c**, Purified Flag–PAC1 complex from fraction 12 was subjected to native-PAGE (**b**) or anion-exchange chromatography (**c**), followed by immunoblotting. **d**, Multistep model of the ordered assembly of mammalian 20S proteasomes. Some of the newly synthesized free α-subunits bind to the PAC1–PAC2 heterodimer, which provides a scaffold for α-ring formation, thereby suppressing the off-pathway aggregation of α-subunits and keeping α-rings competent for half-proteasome formation. Two half-proteasomes then dimerize, the β-subunits are processed and hUmp1 is degraded. The PAC1–PAC2 complex is subsequently degraded by the newly formed active 20S proteasomes.

METHODS

See Supplementary Methods for procedures used in the experiments in Supplementary Figs 1–4.

DNA constructs and cell culture. We synthesized cDNAs encoding PAC1, PAC2, hUmp1 and proteasome α- and β-subunits from total RNA isolated from HeLa cells using Superscript II (Invitrogen). PCR was carried out on the cDNA with Pyrobest DNA polymerase (Takara). All of the amplified fragments were cloned into pcDNA3.1 (Invitrogen) and sequenced for confirmation. For expression of GST fusion proteins, the cDNAs were subcloned into pGEX6P-1 (Amersham). Transfections of 293T cells were done with Fugene 6 (Roche). Stable transfections of HeLa cells or 293T cells were done with Lipofectamine 2000 (Invitrogen), and the cells were selected with 1 mg ml^{-1} of G418 or 5 μg ml^{-1} of puromycin, respectively. We used 20 μM MG132 (Peptide Institute) to inhibit proteasome activities 2 h before the cells were collected.

Protein extracts, immunological analysis and antibodies. Cells were lysed in ice-cold buffer A containing 50 mM Tris-HCl (pH 7.5), 0.5% (v/v) Nonidet P40, 1 mM dithiothreitol (DTT) and 2 mM ATP, and the extracts were clarified by centrifugation at 20,000*g* for 10 min at 4 °C. SDS–PAGE (12% gel or 4–12% gradient Bis-Tris gel; Invitrogen) and native-PAGE (3–8% gradient Tris-acetate gel; Invitrogen) were done in accordance with the manufacturer's instructions. The separated proteins were transferred onto polyvinylidene difluoride membrane and reacted with the indicated antibody. Development was done with Western Lighting reagent (Perkin Elmer). Polyclonal antibodies against hUmp1, PAC1 and PAC2 were raised in rabbits using a synthetic peptide (E_{115}DILNDPSQSE$_{125}$), and recombinant PAC1 and PAC2 protein, respectively. PAC1 and PAC2 were produced and purified as GST fusion proteins, and GST was removed by PreScission protease (Amersham).

Antibodies against proteasome α3 subunit (MCP257), α4 (MCP34), α5 (MCP196), α6 (MCP20), α7 (MCP72), β2 (MCP168) and α-subunits (MCP231, which reacts with all α-subunits except α4) were purchased from BioMol. Antibodies against β5 (P93250), β6 (P93199) and β1i were prepared as described[17]. We used antibodies against the Flag tag (Sigma) and β-actin (Chemicon), and horseradish peroxidase (HRP)-conjugated rabbit anti-mouse and goat anti-rabbit IgG (Jackson ImmunoResearch) for immunodetection. For immunoprecipitation of the Flag epitope, we used M2 agarose (Sigma). For immunoprecipitation of proteasomes, we used antibody MCP34 or MCP20 bound to protein G Sepharose (Amersham). In the experiments in Fig. 1e–f, we used MCP20 crosslinked to NHS-activated Sepharose (Amersham). These beads were added to the extracts, mixed under constant rotation for 2 h at 4 °C, washed four times with buffer A (except in the experiments in Fig. 1e–f), and boiled in SDS sample buffer, or eluted with 100 μg ml^{-1} of Flag peptides (Sigma) or with 0.2 M glycine-HCl (pH 2.8). Densitometric analysis was done with Image Gauge software (Fujifilm). 2D-PAGE was done as described[17].

Glycerol gradient analysis. Samples and molecular weight markers (Amersham) were fractionated by 4–17% (v/v), 4–24% (v/v) or 8–32% (v/v) linear glycerol density gradient centrifugation (22 h, 100,000*g*) as described[17].

Purification of PAC1–PAC2 complex. We coexpressed 3× FLAG–PAC1 and 6× His–PAC2 in *E. coli* using a pRSFDuet-1 vector (Novagen). The cell pellets were lysed in buffer B containing 20 mM sodium phosphate (pH 7.8), 500 mM NaCl and 1.0% Triton X-100, and sonicated. Ni-NTA Sepharose (Qiagen) was added to the extracts, which were then washed with buffer C containing 20 mM sodium phosphate (pH 6.0) and 500 mM NaCl, and eluted with buffer C plus 100 mM imidazole. The eluted products were further purified with M2 agarose and eluted with 100 μg ml^{-1} of Flag peptide (Sigma).

Pulse-chase experiments. Cells were incubated with methionine-free medium for 1 h, metabolically labelled with ^{35}S-methionine for 1 h, and then washed and chased for the indicated time. The cell lysates were immunoprecipitated with M2 agarose, fractionated by SDS–PAGE and visualized by autoradiography.

RNAi experiments. siRNAs targeting human PAC1, PAC2 and hUmp1 with the following 19-nucleotide sequences were designed by B-Bridge and synthesized by Dharmacon: PAC1, 5′-CCAGAAGCUUGAAGGGUUU-3′; PAC2, 5′-GCAUAAAUGCUGAAGUGUA-3′; hUmp1, a mixture of 5′-GCAAGUGG ACCUUUUUGAAA-3′ and 5′-CCUGAGAAUUUCUGCUCAA-3′. Control siRNA (Non-specific Control Duplex VIII) was purchased from B-Bridge. Transfections of siRNAs into HEK293T cells were done with Lipofectamine

2000 at a final concentration of 50 nM in six-well dishes. The cells were analysed 72 h after transfection.

Assay of proteasome activity. Peptidase activity was measured by using a fluorescent peptide substrate, succinyl-Leu-Leu-Val-Tyr-7-amido-4-methyl-coumarin (Suc-LLVY-MCA), as described[27].

Chromatography. Anion-exchange chromatography was done with a Resource Q column (Amersham). Bound proteins were eluted with a salt gradient of 0–1 M NaCl in a buffer containing 50 mM Tris-HCl (pH 8.0), 1 mM DTT and 5% glycerol.

Received 27 June; accepted 2 August 2005.

1. Pickart, C. M. Mechanisms underlying ubiquitination. *Annu. Rev. Biochem.* **70**, 503–533 (2001).
2. Glickman, M. H. & Ciechanover, A. The ubiquitin–proteasome proteolytic pathway: destruction for the sake of construction. *Physiol. Rev.* **82**, 373–428 (2002).
3. Baumeister, W., Walz, J., Zühl, F. & Seemüller, E. The proteasome: paradigm of a self-compartmentalizing protease. *Cell* **92**, 367–380 (1998).
4. Groll, M. *et al.* Structure of 20S proteasome from yeast at 2.4 Å resolution. *Nature* **386**, 463–471 (1997).
5. Unno, M. *et al.* The structure of the mammalian 20S proteasome at 2.75 Å resolution. *Structure (Camb.)* **10**, 609–618 (2002).
6. Zwickl, P., Kleinz, J. & Baumeister, W. Critical elements in proteasome assembly. *Nat. Struct. Biol.* **1**, 765–770 (1994).
7. Gerards, W. L. *et al.* The human α-type proteasomal subunit HsC8 forms a double ringlike structure, but does not assemble into proteasome-like particles with the β-type subunits HsDelta or HsPROS26. *J. Biol. Chem.* **272**, 10080–10086 (1997).
8. Yao, Y. *et al.* α5 subunit in *Trypanosoma brucei* proteasome can self-assemble to form a cylinder of four stacked heptamer rings. *Biochem. J.* **344**, 849–858 (1999).
9. Yang, Y., Truh, K., Ahn, K. & Peterson, P. A. *In vivo* assembly of the proteasomal complexes, implications for antigen processing. *J. Biol. Chem.* **270**, 27687–27694 (1995).
10. Chen, P. & Hochstrasser, M. Autocatalytic subunit processing couples active site formation in the 20S proteasome to completion of assembly. *Cell* **86**, 961–972 (1996).
11. Schmidtke, G. *et al.* Analysis of mammalian 20S proteasome biogenesis: the maturation of β-subunits is an ordered two-step mechanism involving autocatalysis. *EMBO J.* **15**, 6887–6898 (1996).
12. Nandi, D., Woodward, E., Ginsburg, D. B. & Monaco, J. J. Intermediates in the formation of mouse 20S proteasomes: implications for the assembly of precursor β subunits. *EMBO J.* **16**, 5363–5375 (1997).
13. Schmidtke, G., Schmidt, M. & Kloetzel, P. M. Maturation of mammalian 20 S proteasome: purification and characterization of 13 S and 16 S proteasome precursor complexes. *J. Mol. Biol.* **268**, 95–106 (1997).
14. Ramos, P. C., Hockendorff, J., Johnson, E. S., Varshavsky, A. & Dohmen, R. J. Ump1p is required for proper maturation of the 20S proteasome and becomes its substrate upon completion of the assembly. *Cell* **92**, 489–499 (1998).
15. Griffin, T. A., Slack, J. P., McCluskey, T. S., Monaco, J. J. & Colbert, R. A. Identification of proteassemblin, a mammalian homologue of the yeast protein, Ump1p, that is required for normal proteasome assembly. *Mol. Cell. Biol. Res. Commun.* **3**, 212–217 (2000).
16. Witt, E. *et al.* Characterisation of the newly identified human Ump1 homologue POMP and analysis of LMP7(β5i) incorporation into 20 S proteasomes. *J. Mol. Biol.* **301**, 1–9 (2000).
17. Burri, L. *et al.* Identification and characterization of a mammalian protein interacting with 20S proteasome precursors. *Proc. Natl Acad. Sci. USA* **97**, 10348–10353 (2000).
18. Natsume, T. *et al.* A direct nanoflow liquid chromatography-tandem mass spectrometry system for interaction proteomics. *Anal. Chem.* **74**, 4725–4733 (2002).
19. Vidal-Taboada, J. M. *et al.* Down syndrome critical region gene 2: expression during mouse development and in human cell lines indicates a function related to cell proliferation. *Biochem. Biophys. Res. Commun.* **272**, 156–163 (2000).
20. Behar, R. *et al.* Growth retardation, polyploidy, and multinucleation induced by Clast3, a novel cell cycle-regulated protein. *J. Biol. Chem.* **277**, 40012–40019 (2002).
21. Ahn, K. *et al. In vivo* characterization of the proteasome regulator PA28. *J. Biol. Chem.* **271**, 18237–18242 (1996).
22. Tanahashi, N. *et al.* Hybrid proteasomes. Induction by interferon-γ and contribution to ATP-dependent proteolysis. *J. Biol. Chem.* **275**, 14336–14345 (2000).
23. Murata, S. *et al.* Immunoproteasome assembly and antigen presentation in mice lacking both PA28α and PA28β. *EMBO J.* **20**, 5898–5907 (2001).

Supplementary Information is linked to the online version of the paper at www.nature.com/nature.

Acknowledgements We thank Y. Murakami for the ornithine decarboxylase degradation assay system, K. Furuyama for technical support, and D. Finley for comments on the manuscript. This work was supported by grants from the Japanese Science and Technology Agency (to S.M.), the Ministry of Education, Science and Culture of Japan (to S.M. and K.T.) and the New Energy and Industrial Technology Development Organization (to T.N.). Y.H. was supported by the Japanese Society for the Promotion of Science.

Author Information The sequences for human PAC1 and PAC2 have been deposited in GenBank under accession numbers BR000236 and BR000237, respectively. Reprints and permissions information is available at npg.nature.com/reprintsandpermissions. The authors declare no competing financial interests. Correspondence and requests for materials should be addressed to S.M. (smurata@rinshoken.or.jp) or K.T. (tanakak@rinshoken.or.jp).

The EMBO Journal (2006) 25, 554–564 | © 2006 European Molecular Biology Organization | All Rights Reserved 0261-4189/06
www.embojournal.org

THE EMBO JOURNAL

A novel ubiquitin-binding protein ZNF216 functioning in muscle atrophy

Akinori Hishiya[1,2], Shun-ichiro Iemura[3], Tohru Natsume[3], Shinichi Takayama[2], Kyoji Ikeda[1] and Ken Watanabe[1,*]

[1]Department of Bone & Joint Disease, National Center for Geriatrics & Gerontology (NCGG), Obu, Aichi, Japan, [2]Program of Molecular Chaperone Biology, Department of Radiology, Medical College of Georgia, Augusta, GA, USA and [3]Japan Biological Information Research Center (JBIRC), National Institute of Advanced Industrial Science & Technology (AIST), Tokyo, Japan

The ubiquitin–proteasome system (UPS) is critical for specific degradation of cellular proteins and plays a pivotal role on protein breakdown in muscle atrophy. Here, we show that ZNF216 directly binds polyubiquitin chains through its N-terminal A20-type zinc-finger domain and associates with the 26S proteasome. ZNF216 was colocalized with the aggresome, which contains ubiquitinylated proteins and other UPS components. Expression of *Znf216* was increased in both denervation- and fasting-induced muscle atrophy and upregulated by expression of constitutively active FOXO, a master regulator of muscle atrophy. Mice deficient in *Znf216* exhibited resistance to denervation-induced atrophy, and ubiquitinylated proteins markedly accumulated in neurectomized muscle compared to wild-type mice. These data suggest that ZNF216 functions in protein degradation via the UPS and plays a crucial role in muscle atrophy.

The EMBO Journal (2006) **25**, 554–564. doi:10.1038/sj.emboj.7600945; Published online 19 January 2006
Subject Categories: proteins; molecular biology of disease
Keywords: aggresome; muscular atrophy; proteasome; ubiquitin; zinc-finger protein

Introduction

The ubiquitin–proteasome system (UPS) is one of the major protein degradation pathways in eukaryotic cells. The UPS plays key regulatory roles in many cellular processes, including cell cycle control, the regulation of transcription and protein quality control (Hershko and Ciechanover, 1998; Pickart and Cohen, 2004). Aberrations of this system lead to many forms of pathogenesis, such as malignancies, neurodegenerative disease and inflammatory response (Glickman and Ciechanover, 2002). The UPS includes sequential, multistep reactions: ubiquitin-conjugation of target proteins by E1, E2 and E3 enzymes, recognition of ubiquitinylated proteins by ubiquitin-binding proteins or 19S subunits of proteasome and proteolysis in the proteasome.

Many catabolic conditions, such as low-insulin state, hyperthyroidism, sepsis and cancer cachexia lead to enhancement of protein breakdown in skeletal muscle known as muscle atrophy (Mitch and Goldberg, 1996; Lecker *et al*, 1999). In muscle atrophy, the UPS plays a pivotal role in protein breakdown (Price *et al*, 1996; Tawa *et al*, 1997). Several studies indicate that mRNAs encoding UPS components are increased in atrophying muscle (Medina *et al*, 1991; Wing and Goldberg, 1993; Bailey *et al*, 1996; Price *et al*, 1996; Jagoe *et al*, 2002). In particular, the E3 ubiquitin ligases MAFbx/Atrogin-1 and MuRF-1 (muscle RING finger 1) are known to be markers of muscle atrophy (Bodine *et al*, 2001; Gomes *et al*, 2001). Both are induced in multiple models of muscle atrophy including immobilization, denervation and hindlimb suspension, and mice deficient in either gene are resistant to denervation-induced muscle atrophy (Bodine *et al*, 2001). Goldberg and co-workers proposed that atrophy-related genes, whose expression is induced in multiple types of muscle atrophy, are called 'atrogenes' (Sandri *et al*, 2004). Recently, it was demonstrated that the IGF-I/PI3K/Akt pathway is an important regulator of muscle mass in muscle hypertrophy and atrophy (Sacheck *et al*, 2004; Sandri *et al*, 2004; Stitt *et al*, 2004). In that case, the transcription factor FOXO plays a pivotal role in activating atrogenes such as MAFbx/Atrogin-1 (Gomes *et al*, 2001).

Although many UPS players such as E3 ligases have been characterized, the mechanism of how ubiquitinylated proteins are delivered to the proteasome have not been fully elucidated. A component of 19S proteasome, Rpn10/S5a, recognizes the ubiquitinylated proteins (Young *et al*, 1998; Wilkinson *et al*, 2000). It has been shown that yeast proteins, Rad23p and Dsk2p, bind to ubiquitinylated substrates and to the 26S proteasome through their UBA and Ubl domains, respectively, thereby functioning as shuttle proteins that present polyubiquitinylated proteins to the proteasome (Chen *et al*, 2001; Funakoshi *et al*, 2002; Elsasser and Finley, 2005). Loss-of-function of shuttle proteins results in abnormal accumulation of polyubiquitinylated proteins (Lambertson *et al*, 1999; Saeki *et al*, 2002). However, yeast can survive when both *RAD23* and *DSK2* genes are mutated, suggesting that other mechanisms or molecule(s) possessing a shuttle function exist (Saeki *et al*, 2002). Here, we show that ZNF216, a novel ubiquitin-binding protein containing an A20-type zinc-finger, is such a factor. *Znf216* expression is upregulated in skeletal muscle in experimental models of muscle atrophy, and *Znf216*-deficient mice exhibit resistance to muscle atrophy accompanied by abnormal accumulation of polyubiquitinylated proteins in skeletal muscle. Our findings suggest that ZNF216, with its potential function of anchoring ubiquitinylated proteins to the proteasome, plays a critical role in degrading muscle proteins.

*Corresponding author. Department of Bone & Joint Disease, National Center for Geriatrics & Gerontology (NCGG), Obu, Aichi 474-8522, Japan. Tel.: +81 562 46 2311; Fax: +81 562 44 6595;
E-mail: kwatanab@nils.go.jp

Received: 6 June 2005; accepted: 14 December 2005; published online: 19 January 2006